ISTANBUL TECHNICAL UNIVERSITY ★ GRADUATE SCHOOL OF SCIENCE ENGINEERING AND TECHNOLOGY

DESIGN AND IMPLEMENTATION OF BEYOND 5G PHYSICAL LAYER SCHEMES

M.Sc. THESIS

Caner GÖZTEPE

Department of Electronics and Communication Engineering

Telecommunication Engineering Programme

MAY 2019

ISTANBUL TECHNICAL UNIVERSITY ★ GRADUATE SCHOOL OF SCIENCE ENGINEERING AND TECHNOLOGY

DESIGN AND IMPLEMENTATION OF BEYOND 5G PHYSICAL LAYER SCHEMES

M.Sc. THESIS

Caner GÖZTEPE
(504171306)

Department of Electronics and Communication Engineering

Telecommunication Engineering Programme

Thesis Advisor: Prof. Dr. Güneş Karabulut Kurt

MAY 2019

İSTANBUL TEKNİK ÜNİVERSİTESİ ★ FEN BİLİMLERİ ENSTİTÜSÜ

5G SONRASI FİZİKSEL KATMAN ŞEMALARININ TASARIMI VE GERÇEKLEMESİ

YÜKSEK LİSANS TEZİ

Caner GÖZTEPE
(504171306)

Elektronik ve Haberleşme Mühendisliği Anabilim Dalı

Telekomünikasyon Mühendisliği Programı

Tez Danışmanı: Prof. Dr. Güneş Karabulut Kurt

MAYIS 2019

Caner GÖZTEPE, a M.Sc. student of ITU Graduate School of Science Engineering and Technology 504171306 successfully defended the thesis entitled "DESIGN AND IMPLEMENTATION OF BEYOND 5G PHYSICAL LAYER SCHEMES", which he/she prepared after fulfilling the requirements specified in the associated legislations, before the jury whose signatures are below.

Thesis Advisor :	**Prof. Dr. Güneş Karabulut Kurt** Istanbul Technical University	.....
Jury Members :	**Prof. Dr. Hakan Ali Çırpan** Istanbul Technical University	.....
	Dr. Tunçer Baykaş Medipol University	.....
		.....

Date of Submission : **03 May 2019**
Date of Defense : **23 May 2019**

To my family,

FOREWORD

First of all, I would like to thank Prof. Güneş KARABULUT KURT for her invaluable guidance and encouragement throughout my research study. I am thankful to my friends for their precious supports. I would also like to express my profound gratitude to my family due to their precious support and motivation which made this thesis all possible.

May 2019

Caner GÖZTEPE
(Telecommunication Engineer, B.Sc.)

TABLE OF CONTENTS

Page

ABBREVIATIONS

ACI	**:** Adjacent Channel Interference
ADC	**:** Analog to Digital Converter
AS	**:** Antenna Selection
AWGN	**:** Additive White Gaussian Noise
B5G	**:** Beyond $5^{th} generation$
BER	**:** Bit Error Rate
CE	**:** Channel Estimation
CFO	**:** Carrier Frequency Offset
CP-OFDM	**:** Cyclic Prefix Orthogonal Frequency Division Multiplexing
CSI	**:** Channel State Information
DAC	**:** Digital to Analog Converter
DFT	**:** Discrete Fourier Transform
EVM	**:** Error Vector Magnitude
GSM	**:** Generalized Spatial Modulation
ISI	**:** Inter Symbol Interference
MIMO	**:** Multiple Input Multiple Output
NOMA	**:** Non-Orthogonal Multiple Access
QAM	**:** Quadrature Amplitude Modulation
PSD	**:** Power Spectral Density
SDR	**:** Software Defined Radio
SNR	**:** Signal to Noise Ratio
SM	**:** Spatial Modulation
STO	**:** Sample Timing Offset
UF-OFDM	**:** Universal Filtered Orthogonal Frequency Division Multiplexing
USRP	**:** Universal Software Radio Peripheral

SYMBOLS

y	:	Received Signal
h	:	Channel
x	:	Transmitted Signal
α	:	Power Allocation Coefficient
z	:	ACI Component
F	:	Filter Coefficient

LIST OF TABLES

Page

LIST OF FIGURES

Page

DESIGN AND IMPLEMENTATION OF BEYOND 5G PHYSICAL LAYER SCHEMES

SUMMARY

Wireless communication technologies, especially mobile communication technologies which constitute an important part of communication systems reach more and more usage areas. The wide use of mobile communication technologies enables new technology researches to focus on this field. Fourth generation (4G) communication systems which are the latest mobile communication technologies used today, cannot meet the expectations of future users. Therefore, research and development of new technologies continues. For 4G and beyond, researches on the fifth generation (5G) communication systems from different perspectives are made. An important part of the research areas of 5G, which is expected to be clarified in 2020, is the improvement of energy efficiency and spectral efficiency. Different wave-forms and different multiple access techniques are evaluated for 5G in the physical layer where energy efficiency and spectral efficiency can be achieved most. The waveform used in 4G is generally cyclic prefix orthogonal frequency division multiplexing (CP-OFDM) and the multiple access technique used is orthogonal frequency division multiple access (OFDMA). The most important aspects of 5G physical layer research are the development or modification of these techniques to meet user expectations.

The majority of the 5G researches are done in the simulation environment and this is the first step to reach the end user. The new techniques developed are evaluated under a lot of assumptions in the simulation environment. This situation creates an obstacle in front of how fast technologies can adapt to real life. It is impossible for the results obtained in the simulation environment to be exactly the same in real life. Therefore, new technologies developed after simulation must be tested very quickly in real time and must be shown that they can work. For this purpose, software defined radios (SDR) technologies are often used in 5G research. Any system designed in the base band with SDR, can be used easily in real time. As a result of this, new methods can be incorporated into communication systems much faster.

Today where we came to the end of 5G researches, new researches have been started for beyond 5G (B5G). These studies, which will be named B5G throughout the thesis, are carried out to meet the needs of beyond 5G and much more. In the scope this thesis, CP-OFDM and universal filtered orthogonal frequency division multiplexing (UF-OFDM) as different wave-forms, spatial modulation (SM) and generalized spatial modulation (GSM) as different modulation schemes and non-orthogonal multiple access (NOMA) as multiple access technique in the physical layer determined for spectral and energy efficiency were examined from different perspectives in both simulation environment and real time test environment.

General information about the studies carried out within the scope of this thesis and the contributions of the thesis to the literature are explained in Chapter 1.

In Chapter 2, there are explanations about Software Defined Radios and equipment used during the thesis. Software Defined Radios are highly efficient devices in terms of both time and cost in the implementation of communication systems. Therefore, SDR is used in all studies conducted during the thesis phase. An overview of the SDR technology and the SDR equipment used is given in Chapter 2 in detail.

One of the multiple access techniques, NOMA is evaluated in Chapter 3. NOMA can use the same frequency band to serve multiple users in the same time frame. This is a good solution to the increase the number of users and also it is a very effective method in terms of spectrum efficiency. Within the scope of this thesis, NOMA system with the relay in the power zone was first examined in the real time test environment in the literature. NOMA's with and without relay performances have been evaluated in both simulation and real time testing environment in the created test environment. The pros and cons of the use of the relay are described in the study.

In Chapter 4, one of the multi-carrier wave-forms, UF-OFDM is recommended to eliminate some of the deficiencies of CP-OFDM. UF-OFDM (also known as UFMC) reduces synchronization problems, which are negative features of CP-OFDM, and reduces the spectral efficiency. It is a successful waveform recommended to eliminate side-band overflows. UF-OFDM makes CP-OFDM more stable with the help of filtering. UF-OFDM has similar performances according to filter bank multicarrier (FBMC) or generalized frequency division multiplexing (GFDM) techniques, which are recommended in the literature and it is a much easier method to implement together. Besides, as UF-OFDM and CP-OFDM systems are very similar to each other, convenience can be provided for UF-OFDM's compliance with the systems used. In the studies conducted within the scope of the thesis, it has been shown that when UF-OFDM is used, no need for protection band which is mandatory to use due to CP-OFDM's side bands. In the studies conducted in both simulation environment and real time testing environment, CP-OFDM and UF-OFDM were compared in single input single output (SISO) and single input multiple output (SIMO) communication systems. In the generated scenario, it has been shown that CP-OFDM definitely needs protection band. It was determined that UF-OFDM's protection band need is much less than CP-OFDM and thus it can provide spectral efficiency.

SM and GSM using single-carrier waveforms are examined in chapters 5 and 6, respectively. Spatial modulation is a modulation technique that uses a single-carrier modulation scheme and is highly prominent in both spectral and energy efficiency. In spatial modulation, a single RF chain is used as hardware on the transmitter. As a result of reducing the number of antenna index against information bits depending on the number of antennas, more bits can be sent from the same channel. These two conditions make SM very efficient in energy and spectral efficiency. In the studies conducted within the scope of the thesis, SM technique was performed for the first time in the literature in the massive multiple input multiple output (MIMO) system with 16x4 antenna. In order to improve the error performance, the optimum method, EDAS, was applied in both simulation environment and real time test environment and its effect on error performance was determined. Within the scope of the thesis, k nearest neighborhood (k-NN) method, which is one of the machine learning algorithms, is suggested instead of Euclidean distance antenna selection (EDAS) used in communication systems. EDAS and k-NN were compared in simulation environment and real time test environment in terms of performance. It has been

observed that k-NN method gives better results in terms of error performance in real time.

Unlike the spatial modulation scheme, generalized spatial modulation contains more than one RF chain on the transmitter. Therefore, as a result of reduction of each different antenna combination being used against different index bits, in most cases more information bits can be sent from SM. In the studies conducted within the scope of the thesis, the GSM system was realized the first time in the literature. For this purpose, a MIMO system creation with 16x4 antenna was realized. The performance of GSM system was evaluated by using two different antennas at the same time in the transmitter. In order to improve the error performance, the recommended optimum method, EDAS, was examined in both the simulation and real time testing environment under perfect and imperfect channel state information (CSI). In case of imperfect CSI, one of the machine learning algorithms, decision tree (DT) and multi-layer perceptrons (MLP) have been suggested instead of EDAS, which cannot achieve the desired performance. For the first time in the literature, the recommended machine learning algorithms were used in real time testing system as with real time. According to the results, the recommended algorithms showed more successful error performance than EDAS under imperfect CSI.

Finally, in Chapter 7, the general information and results of the thesis are evaluated. Some recommendations are presented.

5G SONRASI FİZİKSEL KATMAN ŞEMALARININ TASARIMI VE GERÇEKLEMESİ

ÖZET

Haberleşme sistemlerinin önemli bir bölümünü oluşturan kablosuz haberleşme ve özellikle mobil haberleşme teknolojileri, gün geçtikçe daha fazla kullanım alanına ulaşmaktadırlar. Mobil haberleşme teknolojilerinin çokça kullanımı, yeni teknoloji araştırmalarının da bu alana yoğunlaşmasını sağlamaktadır. Günümüzde kullanılan en son mobil haberleşme teknolojileri olan 4. nesil (4G) haberleşme sistemleri, gelecekteki kullanıcı beklentilerini karşılayamamakta ve bu nedenle yeni teknolojilerin araştırılmasına ve geliştirilmesine devam edilmektedir. 4G sonrası için, 5. nesil (5G) haberleşme sistemleri üzerine oldukça farklı perspektiflerden araştırmalar yapılmaktadır. 2020 yılında netleşmesi beklenen 5G'nin araştırma alanlarının önemli bir bölümünü, enerji verimliliğinin ve spektrum verimliliğinin arttırılması oluşturmaktadır. Enerji verimliliği ve spektrum verimliliğinin en çok elde edilebileceği katman olan fiziksel katmanda, farklı dalga formları ve farklı çoklu erişim teknikleri 5G için değerlendirilmektedir. 4G'de, kullanılan dalga formu genel olarak cyclic prefix orthogonal frequency division multiplexing (CP-OFDM) ve çoklu erişim tekniği orthogonal frequency division multiple access (OFDMA)'dır. Fiziksel katman 5G araştırmalarının en önemli konuları, bu tekniklerin kullanıcı beklentilerini karşılayabilmek amacıyla geliştirilmesi ya da değiştirilmesidir.

5G araştırmalarının çoğunluğu itibariyle benzetim ortamında yapılması, son kullanıcıya ulaşmasının ilk aşamasıdır. Geliştirilen yeni teknikler, benzetim ortamında çok fazla varsayım altında değerlendirilmektedir. Bu durum da teknolojilerin gerçek hayata ne kadar hızlı uyum sağlayabileceğinin önünde bir engel teşkil etmektedir. Benzetim ortamında elde edilen sonuçların gerçek hayatta birebir olması imkânsızdır. Bu nedenle benzetim sonrasında geliştirilen yeni teknolojilerin çok hızlı bir şekilde gerçek zamanda test edilmesi ve çalışabilir olduğunun gösterilmesi gerekmektedir. Bu amaçla, sıklıkla, SDR teknolojileri 5G araştırmalarında kullanılmaktadır. SDR'lar ile temel bantta tasarlanan herhangi bir sistem, kolaylıkla gerçek zamanda kullanılabilmektedir. Bunun sonucu olarak, geliştirilen yeni yöntemlerin çok daha hızlı bir şekilde haberleşme sistemlerine dâhil olması sağlanabilmektedir.

5G araştırmalarının sonuna gelindiği günümüzde, 5G sonrası için de yeni araştırmalara başlanmıştır. Tez boyunca da beyond 5G (B5G) olarak adlandırılacak bu çalışmalar, 5G'nin çok daha ilerisindeki ihtiyaçların karşılanması amacıyla yapılmaktadır. Bu tez kapsamında, spektrum verimliliği ve enerji verimliliği amacıyla belirlenen fiziksel katmandaki farklı dalga formları ve çoklu erişim teknikleri hem benzetim ortamında hem de gerçek zaman test ortamında farklı perspektiflerden araştırılmıştır. Bu tez kapsamında incelenen teknikler, takip eden bölümlerde detaylandırılmaktadır.

Bu tez kapsamında yapılan çalışmalar ile ilgili genel bir bilgilendirme ve tezin literatüre katkıları Birinci Bölümde anlatılmaktadır.

İkinci Bölümde yazılım tabanlı radyolar ve tez süresince kullanılan ekipmanlar ile ilgili açıklamalar bulunmaktadır. Yazılım tabanlı radyolar, haberleşme sistemlerinin gerçekleştirilmesinde hem zaman hem de maliyet açısından oldukça verimli cihazlardır. Bu nedenle, tez aşamasında gerçekleştirilen tüm çalışmalarda SDR'lar da kullanılmıştır. SDR teknolojisi hakkında özet bir bilgi ve kullanılan SDR donanımları detaylı bir şekilde bölüm 2'de verilmektedir.

Çoklu erişim tekniklerinden NOMA, Üçüncü Bölümde değerlendirilmektedir. Aynı zaman diliminde, aynı frekans bandını birden fazla kullanıcıya hizmet verecek şekilde kullanabilen NOMA, kullanıcı sayısındaki artış için iyi bir çözüm olmakla birlikte spektrum verimliliği bakımından da oldukça etkili bir yöntemdir. Bu tez kapsamında, güç bölgesinde oluşturulan röleli NOMA sistemi literatürde ilk kez gerçek zaman test ortamında incelenmiştir. Tasarlanan test ortamında, NOMA'nın rölesiz ve röleli başarımları, hem benzetim hem de gerçek zaman test ortamında değerlendirilmiştir. Röle kullanımının artıları ve eksikleri çalışma kapsamında açıklanmaktadır.

Dördüncü Bölümde, çok taşıyıcı dalga formlarından UF-OFDM, CP-OFDM'nin bazı eksikliklerini gidermek amacıyla önerilmektedir. UF-OFDM (ya da UFMC), CP-OFDM'nin olumsuz özelliklerinden olan senkronizasyon problemlerini ve spektrum verimliliğini azaltan, yan bant taşmalarını gidermek amacıyla önerilen başarılı bir dalga formudur. UF-OFDM, filtreleme yardımıyla, CP-OFDM'yi daha kararlı hale getirmektedir. UF-OFDM, literatürde önerilen filtreleme uygulamalarından FBMC ya da GFDM tekniklerine göre benzer performanslara sahip olmakla birlikte gerçeklemesi çok daha kolay bir yöntemdir. Ayrıca, UF-OFDM ve CP-OFDM sistemleri birbirine oldukça benzer olduğundan, UF-OFDM'nin kullanılan sistemlere uyumunda kolaylık sağlanabilecektir. Tez kapsamında gerçekleştirilen çalışmalarda, CP-OFDM'nin yan bantlarından dolayı kullanılması zorunlu olan koruma bandına, UF-OFDM kullanıldığı durumda gerek olmadığı gösterilmiştir. Hem benzetim ortamında hem gerçek zaman test ortamında gerçekleştirilen çalışmalarda SISO ve SIMO haberleşme sistemlerinde CP-OFDM ve UF-OFDM karşılaştırılmıştır. Oluşturulan senaryoda, CP-OFDM'nin kesinlikle koruma bandına ihtiyacı olduğu gösterilmiştir. UF-OFDM'nin ise koruma bandı ihtiyacının CP-OFDM'ye göre çok daha az olduğu ve böylelikle spektrum verimliliği sağlayabileceği belirlenmiştir.

Tek taşıyıcılı dalga formu kullanan SM ve GSM sırasıyla Beşinci ve Altıncı Bölümlerde incelenmektedir. Uzaysal modülasyon, tek taşıyıcılı modülasyon şeması kullanan ve hem spektrum hem de enerji verimliliği bakımından oldukça ön planda bulunan bir modülasyon tekniğidir. Uzaysal modülasyonda, vericide donanımsal olarak tek bir RF zinciri kullanılmaktadır. Anten sayısına bağlı olarak farklı anten indislerinin bilgi bitlerine karşı düşürülmesi sonucu aynı kanaldan, daha fazla bit gönderilebilmektedir. Bu iki durum, SM'nin enerji ve spektrum verimliliğinde oldukça verimli olmasını sağlamaktadır. Tez kapsamında gerçekleştirilen çalışmalarda, SM tekniği, literatürde ilk kez, 16x4 antenli masif MIMO sisteminde gerçeklenmiştir. Hata performansını iyileştirmek amacıyla optimum yöntem olan EDAS, hem benzetim ortamında hem de gerçek zaman test ortamında uygulanarak hata başarımı üzerine etkisi belirlenmiştir. Tez kapsamında, makine öğrenmesi algoritmalarından k-NN yöntemi, haberleşme sistemlerinde kullanılan EDAS yerine önerilmiştir. Performans bakımından EDAS ile k-NN, benzetim ortamında ve gerçek zaman test ortamında karşılaştırılmıştır. Gerçek zamanda, k-NN yönteminin hata performansı bakımından daha iyi sonuç verdiği gösterilmiştir.

Genelleştirilmiş uzaysal modülasyon, uzaysal modülasyon şemasından farklı olarak vericide birden fazla RF zincir içermektedir. Bu nedenle, kullanılan her farklı anten kombinasyonunun, farklı indis bitlerine karşı düşürülmesi sonucu, çoğu durumda SM'den daha fazla bilgi biti gönderilebilmektedir. Tez kapsamında gerçekleştirilen çalışmalarda, literatürde ilk kez GSM sistem gerçeklemesi yapılmıştır. Bu amaçla, 16x4 antenli MIMO bir sistem tasarımı gerçekleştirilmiştir. Vericide iki farklı anten aynı anda kullanılarak, GSM sisteminin başarımı değerlendirilmiştir. Hata performansını iyileştirmek amacıyla önerilen optimum yöntem olan EDAS, hem benzetim hem de gerçek zaman test ortamında perfect ve Imperfect CSI altında araştırılmıştır. Imperfect CSI durumunda, istenilen başarımı sağlayamayan EDAS yerine makine öğrenmesi algoritmalarından decision tree (DT) ve Multi-Layer Perceptrons (MLP) önerilmiştir. Literatürde ilk kez, önerilen makine öğrenmesi algoritmaları gerçek zamanlı olarak, gerçek zaman test sisteminde kullanılmıştır. Elde edilen sonuçlara göre önerilen algoritmalar, imperfect CSI altında EDAS'tan daha başarılı hata performansları göstermişlerdir.

Son olarak, Yedinci Bölüm'de, tez ile ilgili genel bilgiler ve sonuçlar değerlendirilmektedir. Bu tez sonrası ile ilgili bazı tavsiyeler sunulmaktadır.

1. INTRODUCTION

Wireless communication technologies, especially mobile communication technologies which constitute an important part of communication systems reach more and more usage areas. The wide use of mobile communication technologies enables new technology researches to focus on this field. Fourth generation (4G) communication systems which are the latest mobile communication technologies used today, cannot meet the expectations of future users. Therefore, research and development of new technologies continues. For 4G and beyond, researches on the fifth generation (5G) communication systems from different perspectives are made. An important part of the research areas of 5G, which is expected to be clarified in 2020, is the improvement of energy efficiency and spectral efficiency. Different wave-forms and different multiple access techniques are evaluated for 5G in the physical layer where energy efficiency and spectral efficiency can be achieved most. The waveform used in 4G is generally cyclic prefix orthogonal frequency division multiplexing (CP-OFDM) and the multiple access technique used is orthogonal frequency division multiple access (OFDMA). The most important aspects of 5G physical layer research are the development or modification of these techniques to meet user expectations.

Some expectations of 5G technology can be listed as follows [1]:

- In theory, 10Gbps speed (10-100 times better than 4G).
- Maximum 1ms delay (10 times better than 4G).
- 1000 times more bandwidth than 4G in unit area.
- At least 100 billion connectable devices.
- Almost seamless and continuous communication.
- Coverage of the whole world. 9 times lower power consumption.
- 10-year sustainability in low power consumption in machine-type devices.

- High spectral efficiency.

The majority of the 5G researches are done in the simulation environment and this is the first step to reach the end user. The new techniques developed are evaluated under a lot of assumptions in the simulation environment. This situation creates an obstacle in front of how fast technologies can adapt to real life. It is impossible for the results obtained in the simulation environment to be exactly the same in real life. Therefore, new technologies developed after simulation must be tested very quickly in real-time and must be shown that they can work. For this purpose, software defined radios (SDR) technologies are often used in 5G research. Any system designed in the base band with SDR, can be used easily in real-time. As a result of this, new methods can be incorporated into communication systems much faster.

Today where we came to the end of 5G researches, new researches have been started for beyond 5G (B5G). These studies, which will be named B5G throughout the thesis, are carried out to meet the needs of beyond 5G and much more. In the scope of this thesis, CP-OFDM and universal filtered orthogonal frequency division multiplexing (UF-OFDM) as different wave-forms, spatial modulation (SM) and generalized spatial modulation (GSM) as different modulation schemes and non-orthogonal multiple access (NOMA) as multiple access technique in the physical layer determined for spectral and energy efficiency were examined from different perspectives in both simulation environment and real-time test environment.

The rest of this thesis is organized as follows. In Chapter 2, there are explanations about Software Defined Radios and equipment used during the thesis. One of the multiple access techniques, NOMA is evaluated in Chapter 3. In Chapter 4, one of the multicarrier wave-forms, UF-OFDM is recommended to eliminate some of the deficiencies of CP-OFDM. SM and GSM using single-carrier waveforms are examined in chapters 5 and 6, respectively. Finally, in Chapter 8, the general information and results of the thesis are evaluated. Some recommendations are presented.

1.1 Contributions

The contributions of the methods presented and evaluated in this thesis to the literature are shared in this section.

1.1.1 NOMA

NOMA can use the same frequency band to serve multiple users in the same time frame. This is a good solution to the increase the number of users and also it is a very effective method in terms of spectral efficiency. Within the scope of this thesis, NOMA system with the relay in the power zone was first examined in the real-time test environment in the literature. NOMA's with and without relay performances have been evaluated in both simulation and real-time testing environment in the created test environment. The pros and cons of the use of the relay are described in the study.

1.1.2 UF-OFDM

UF-OFDM is recommended to eliminate some of the deficiencies of CP-OFDM. UF-OFDM (also known as UFMC) reduces synchronization problems, which are negative features of CP-OFDM, and reduces the spectral efficiency. It is a successful waveform recommended to eliminate side-band overflows. UF-OFDM makes CP-OFDM more stable with the help of filtering. UF-OFDM has similar performances according to filter bank multicarrier (FBMC) or generalized frequency division multiplexing (GFDM) techniques, which are recommended in the literature and it is a much easier method to implement together. Besides, as UF-OFDM and CP-OFDM systems are very similar to each other, convenience can be provided for UF-OFDM's compliance with the systems used. In the studies conducted within the scope of the thesis, it has been shown that when UF-OFDM is used, no need for protection band which is mandatory to use due to CP-OFDM's side bands. In the studies conducted in both simulation environment and real-time testing environment, CP-OFDM and UF-OFDM were compared in single input single output (SISO) and single input multiple output (SIMO) communication systems. In the generated scenario, it has been shown that CP-OFDM definitely needs protection band. It was determined that UF-OFDM's protection band need is much less than CP-OFDM and thus it can provide spectral efficiency.

1.1.3 SM

Spatial modulation is a modulation technique that uses a single-carrier modulation scheme and is highly prominent in both spectral and energy efficiency. In spatial

modulation, a single RF chain is used as hardware on the transmitter. As a result of reducing the number of antenna index against information bits depending on the number of antennas, more bits can be sent from the same channel. These two conditions make SM very efficient in energy and spectral efficiency. In the studies conducted within the scope of the thesis, SM technique was performed for the first time in the literature in the massive multiple input multiple output (MIMO) system with 16x4 antenna. In order to improve the error performance, the optimum method, EDAS, was applied in both simulation environment and real-time test environment and its effect on error performance was determined. Within the scope of the thesis, k nearest neighborhood (k-NN) method, which is one of the machine learning algorithms, is suggested instead of Euclidean distance antenna selection (EDAS) used in communication systems. EDAS and k-NN were compared in simulation environment and real-time test environment in terms of performance. It has been observed that k-NN method gives better results in terms of error performance in real-time.

1.1.4 GSM

Unlike the spatial modulation scheme, generalized spatial modulation contains more than one RF chain on the transmitter. Therefore, as a result of reduction of each different antenna combination being used against different index bits, in most cases more information bits can be sent from SM. In the studies conducted within the scope of the thesis, the GSM system was realized the first time in the literature. For this purpose, a MIMO system creation with 16x4 antenna was realized. The performance of GSM system was evaluated by using two different antennas at the same time in the transmitter. In order to improve the error performance, the recommended optimum method, EDAS, was examined in both the simulation and real-time testing environment under perfect and imperfect channel state information (CSI). In case of imperfect CSI, one of the machine learning algorithms, decision tree (DT) and multi-layer perceptrons (MLP) have been suggested instead of EDAS, which cannot achieve the desired performance. For the first time in the literature, the recommended machine learning algorithms were used in real-time testing system as with real-time. According

to the results, the recommended algorithms showed more successful error performance than EDAS under imperfect CSI.

1.2 Outline

Explanations about the inputs and contributions were made in the first part of this thesis which is evaluated from the perspective of spectral and energy efficiency of 5G and beyond 5G communication systems. In Chapter 2, general information about the software defined radios used throughout the thesis and the devices used are explained. NOMA system design and test results with and without relay are detailed in Chapter 3. Chapter 4 describes the studies on CP-OFDM and UF-OFDM. Chapter 5 and Chapter 6 describe the SM and GSM systems, respectively. In Chapter 7, the results of the thesis study are generally evaluated and some recommendations for future studies are recommended.

2. SOFTWARE DEFINED RADIO

Mobile communication is among the most widely used wireless communication technologies today. In particular, the development of long term evolution (LTE) technology has resulted in significant increases in spectral efficiency and data speed. Ease of use and day-to-day development of more successful communication technologies are leading to an increase in usage rate and an increase in expectation. The increase of internet of things (IoT) applications also increases the need for use considerably. The necessity of today's technology to meet and develop future expectations is accompanied by the search for new technology.

Thanks to the software defined radios used for the rapid application of new technologies, new developed methods can be tested quickly in real-time environment. Although the design cost of communication systems is very low in the simulation environment, the hardware implementation is quite expensive. This situation also slows down the progress of communication technologies. The most important effect of the use of the SDR is emerging here. Software defined radios enable the real-time testing of any communication system designed in the base-band, much more realistic than the simulation environment with the help of analog to digital converter (ADC), digital to analog converter (DAC), local oscillator and various filters within themselves.

Block diagram of the basic software defined radio system is shown in Figure 2.1.

As detailed in [2], some features of SDR that should be considered are summarized as follows:

- Hardware-Software Decomposition: When a separation is made between the software in use and the hardware used, without the designer having to deal with system complexity, necessary technical details of the equipment can be more understandable and system design can be simplified. The scope of hardware and software decomposition should be made in a wide range in all layers of communication systems.

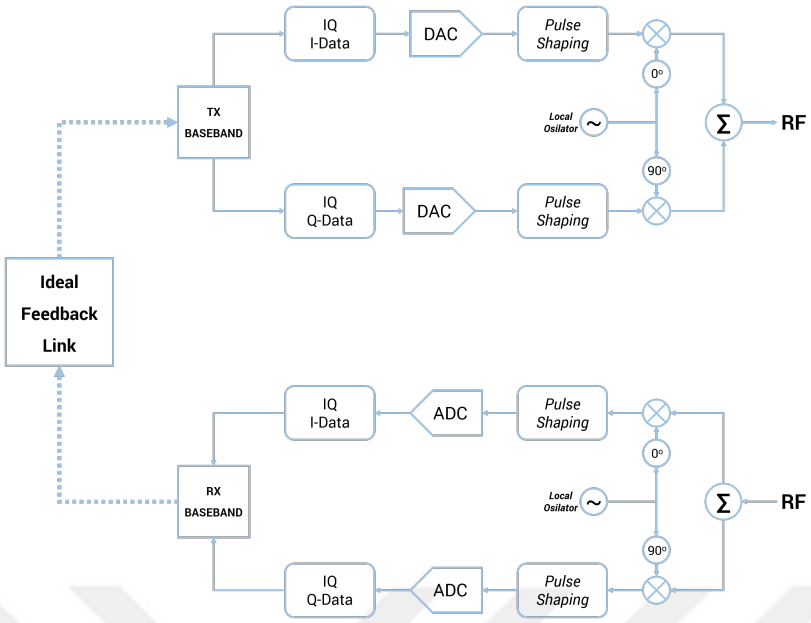

Figure 2.1 : Software defined radio block diagram.

- Comprehensive Software Development Environments: System design applications with SDR should include heterogeneous processing components and different calculation algorithms.In this way, design, development and optimization of a system can be achieved by using appropriate tools and methods. The software tools used for SDR management must be able to combine the simulation environment with the real-time testing environment. Besides, it is a must that the data processing speed of the software should be quite high.

- Different Hardware Integration: The software tools used in the SDR system should support different hardware, interfaces and libraries. During the common use of different hardware and libraries, there should be no problem due to the software used.

In software defined radios, designs are made in software application environment. All communication systems made in computer environment, can be used in real-time by using the desired carrier frequency and bandwidth. During this study, USRP devices, which are often preferred as SDR used, and LabVIEW is used as the software for managing these devices.

LabVIEW is a visual programming language that differs from traditional text-based programming languages. LabVIEW programs consists of two parts, the front panel,

where systems are managed and seen by users and the block diagram which is formed by schemes where systems are designed. Although USRP is generally used in research laboratories, they can also be preferred for different purposes.

2.1 Measurement System

In this study, various wave-forms, various modulation schemes and various multiple access techniques were tested using SDRs. During the tests, SISO, SIMO and MIMO communication systems were designed.

SISO and SIMO test-beds are realized with NI USRP-2921 nodes, NI PXIe-5644 PXI Vector Signal Transceiver and NI PXI-6683H module. USRP-2921 devices are SDR nodes which are functional in 2.4-2.5 and 4.9-5.9 GHz bands and can offer 20 MHz bandwidth as well as 100 million samples per second. These devices are congured as a transmitter and a receiver. For synchronization of the system, PXI-6683H timing and synchronization module is used. This module provides 10 MHz clock signal which is transmitted to nodes with RF cables and is capable of 1 ppm synchronization via TCXO oscillator. With corresponding software conguration, synchronization solution is prepared with these components. NI PXIe-1082 PXI-Chassis and NI PXI-8135 embedded controller are used for manage USRPs and the other modules.

MIMO test-bed is realized with eight NI USRP-2943Rs, two NI USRP-2940s, two NI CDA-2990 octaclock, NI PXIe-6674T timing module and NI CPS-8910 Switch Device for PCI Express. The USRP-2943R has two RF chains and operates in the 1.2GHz to 6GHz range. It is used as a transmitter with a maximum power of 20 dBm and as a receiver with a power of -15 dBm. It has 40 MHz bandwidth. The maximum I/Q sample rate is 200 MS/s. The spurious free dynamic range (sFDR) on the transmitter is 80 dB and on the the receiver sFDR is 88dB. USRP-2940 has two different RF chains. It works as a transmitter with a maximum power of 20 dBm and as a receiver with a power of -15 dBm in the range of 50 MHz and 2.2 GHz. Except from operating frequency, it has similar characteristics with USRP-2943R. The CDA-2990 is the most basic equipment for generating and distributing 8-channel PPS and reference symbols and providing synchronization in the MIMO system design. It is distributed to USRP-2943R by being multiplexed with the reference symbol CDA-2990 and with PPS provided from the NI PXIe-6674T module. USRP 2943R

devices can be combined and controlled via a single channel with NI CPS-8910 Switch Device. All modules and devices are managed with MIMO test-bed, NI PXIe-1085 and NI PXIe-8135.

3. NOMA

3.1 Introduction

Along with the increase in the number of users and the diversity of wireless communication systems, it has become necessary to use the same frequency band of different applications and users. Non-orthogonal multiple access (NOMA), which allows multiple users to share the same frequency band in the same time frame, is projected as a promising multiple access candidate for the fifth generation (5G) and beyond 5G mobile communication systems [3]. Many theoretical studies demonstrate the efficiency of NOMA techniques to design resource and power allocation algorithms, modulation and coding schemes for multi-user uplink and downlink transmissions [4] - [5]. NOMA techniques are divided into two categories as power domain NOMA and code domain NOMA. This study refers to generally preferred the power domain NOMA. In the power domain NOMA, different power coefficients are allocated to different users according to the channel state information (CSI) in order to achieve high system performance with the so-called super position coding (SC), signals from multiple users are superimposed on the transmitter. On the receiver side, the signals are separated from each other by applying successive interference cancellation (SIC) until the users' signal is obtained.

NOMA provides superior spectrum efficiency with the SIC used in the receiver and the SC in the transmitter [4]. However, interventions between users may not be completely eliminated in the SIC process due to erroneous decisions caused by channels. In [6], a definite closed form bit error rate (BER) expression is derived in the presence of SIC errors for both downlink and uplink NOMA schemes in Rayleigh fading channels. On the other hand, power domain NOMA can be implemented in a simple way since it does not require significant changes in existing networks. Furthermore, no additional bandwidth is required to increase spectral efficiency (SE) [7]. So far, although most of the studies on NOMA are concentrated on theoretical analysis and simulation, studies aiming at real-time implementation of NOMA have started to take place in the

literature. In [8], downlink NOMA was implemented in software defined radio (SDR) nodes to assess performance differences between NOMA and orthogonal multiple access (OMA) techniques. In addition, the authors modified the long term evaluation (LTE) protocols set in accordance with NOMA. The results obtained in the experiments show the performance advantages of NOMA with respect to OMA. In [5], detailed comparisons were made between comprehensive computer simulations in OMA and NOMA methods. In NOMA, single user multiple input multiple output (SU-MIMO) system is integrated for downlink and uplink transmission. Besides, a test environment has been created for downlink NOMA and NOMA performance has been investigated under real-time disturbances with the SU-MIMO system. In [9], it has been seen that one of the most important challenges for implementing a practical NOMA system is the complexity of the SIC receiver. Using the SDR nodes, the time consumption of each process step in the SIC receiver is calculated, and the time consumption is extended and cannot work in real-time when the bandwidth increases. In the traditional NOMA, the issue of unbalanced power allocation, seen as a performance-limiting factor, is discussed in [10]. The authors propose network coded multiple access (NCMA) in NOMA using physical layer network coding (PNC). It was confirmed by experimental results that the proposed NCMA systems provide a noticeable performance increase in scenarios where power is balanced. In [11], the NOMA system was moved to mini computers to develop a portable NOMA based test platform based on SDR nodes. A series of experiments have been conducted comparing this portable platform with the desktop NOMA system. As a result, performance loss of more than %12 was observed. In addition to these studies; the literature presents an uncommon uplink NOMA system application in [12]. In the study, a new NOMA design has been proposed for uplink NOMA users to be used for time synchronization and channel estimation of the system.

In contrast to the studies in the literature, downlink system realization of power domain NOMA was performed in SDR nodes in this chapter. Furthermore, the BER values of the relay and the source according to the transmitter gains were examined by adding the relay to the system. The rest of the study is organized as follows: the NOMA system model and the relay system are described in section 3.2. Section 3.3 describes the NOMA test setup performed on SDR nodes. The test results are presented in

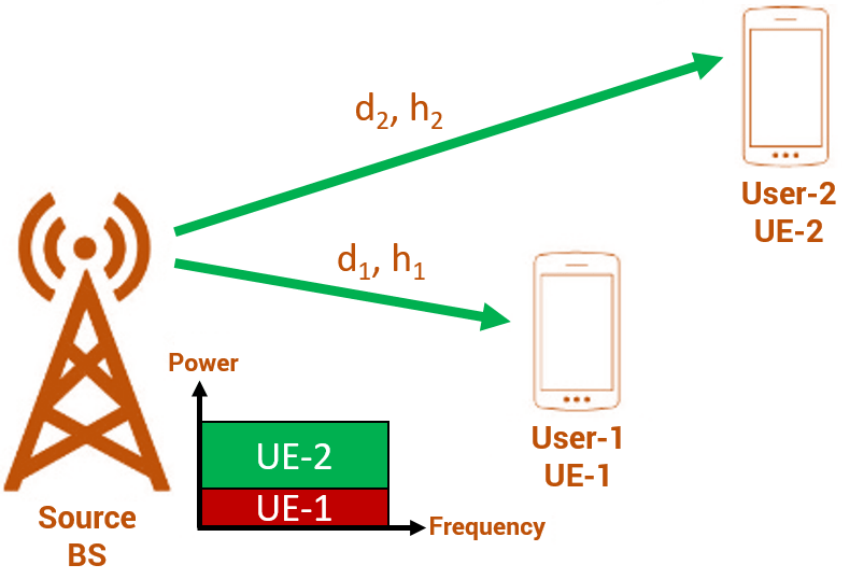

Figure 3.1 : Downlink NOMA system model.

section 3.4. Finally, section 3.5 concludes the article and evaluates the significant results obtained in this section.

3.2 System Model

The system used in this study consists of a base station (BS) as a source node, a relay node and two user nodes. It is assumed that one of the users is close to the source called close user (UE_1), the other is near the edge of the cell called remote user (UE_2). All of the nodes have a single antenna, except the relay node with two antennas, and there is a downlink transmission from source to users.

3.2.1 NOMA without relay

Figure 3.1 shows a two-user downlink NOMA system model. d_k refers to the distance of users to the source, and h_k is the channel gain of users where $k \in \{1,2\}$ represents user id and $|h_2|^2 < |\mathrm{h}_1|^2$.$The symbols produced for \mathrm{UE}_1$ is are x_1 and UE_2 is are x_2 are superimposed on the source side so that the transmitted symbol x is

$$x = \sqrt{\alpha P_t} x_1 + \sqrt{(1-\alpha) P_t} x_2, \tag{3.1}$$

according to the determined power allocation coefficients. The power of the transmitter is A5. The power allocation coefficients of UE_1 and UE_2 are α and $1-\alpha$,

respectively. In this study, the method that channel gains and power allocation coefficients are inversely proportional is used from different power allocation coefficient techniques.Thus, the user, has the lower channel gain, takes more power. This is achieved by selecting $\alpha < 0.5$.

The signal y_k received by the users after passing through the wireless channels is

$$y_k = h_k(\sqrt{\alpha P_t}x_1 + \sqrt{(1-\alpha)P_t}x_2) + n_k \tag{3.2}$$

where $k \in \{1,2\}$. h_k is the channel gain and n_k is the noise component. Before UE_1 decodes its own signal, the signal of UE_2 must be detected bu UE_1. UE_1 removes the signal of US_2 from the received signal. This application is called the SIC process. In this study, a SIC scheme is preferred at the code word level because it performs better than the symbol level SIC.

First, the bit sequence of UE_2 is obtained from the signal received by channel equalization and demodulation. Then, this bit sequence is re-modulated to obtain the symbols of UE_2. The symbols obtained for the cancellation of the signal of UE_2 are again multiplied by the power allocation coefficient and subtracted from the received signal and divided by the power allocation coefficient of UE_1 to obtain the signal of UE_1.

$$\tilde{x_1} = \frac{\tilde{x} - \sqrt{1-\alpha}\tilde{x_2}}{\sqrt{\alpha}} \tag{3.3}$$

In the UE_2 receiver, SIC is not applied and the received signals are demodulated directly. Because the signal strength of UE_1 is lower, the signal belonging to UE_1 in UE_2 receiver is perceived as noise and can decode its own code from y_2.

3.2.2 NOMA with relay

Figure 3.2 shows the scenario in which transmission between the source and users is provided with the help of a relay. The relay is bi-directional and therefore has two different antennas to receive and transmit signals. It is assumed that the relay does not create interference. In addition, it is assumed that the relay uses the amplify and forward method to re-transmit signals and therefore does not decode NOMA users'

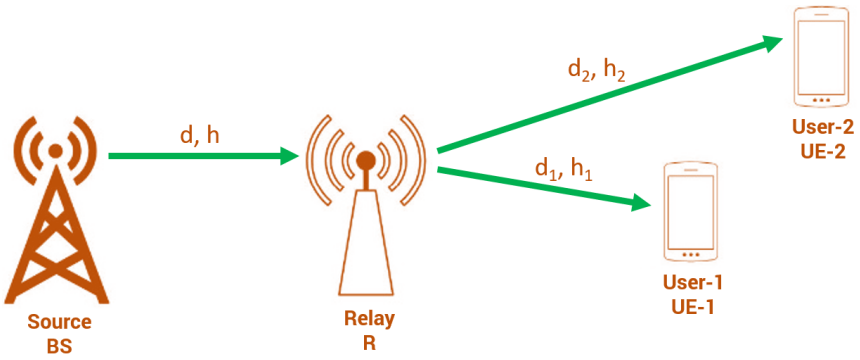

Figure 3.2 : Downlink NOMA with relay system model.

Table 3.1 : System parameters.

Parameters		**Value**
Carrier Frequency		1.2 GHz
Bandwidth		1 MHz
I/Q Rate		1 MS/s
Modulation		4-QAM
Power Allocation Factor		0.2 / 0.8
Source TX Gain		1 - 9 dB
Distance to Source	UE-1	1 m
	UE-2	2 m
Receiver Gain	UE-1	10 dB
	UE-2	10 dB

signals. In this method, the relay node multiply the received signal that brings it to normalized power and then sends it to users. In this scenario, it is assumed that there is no direct connection between the source and the users because of the long distance or obstacles between them. The signal y_k transmitted by the relay is

$$y_k = h_k(h_0(\sqrt{\alpha P_t}x_1 + \sqrt{(1-\alpha)P_t}x_2) + n_0) + n_k \tag{3.4}$$

where $k \in \{1,2\}$ and h_0 is the channel gain between the source node and the relay node and n_0 is the noise component in this channel.

3.3 Test-bed

SDR nodes were used to design the NOMA system model in a real-time test environment. In this system, there are 4 universal serial radio peripheral (USRP) nodes are used as a SDR including 1 source, 2 user and 1 relay nodes. The experimental test-bed generated by USRP nodes is shown in Figure 3.3.

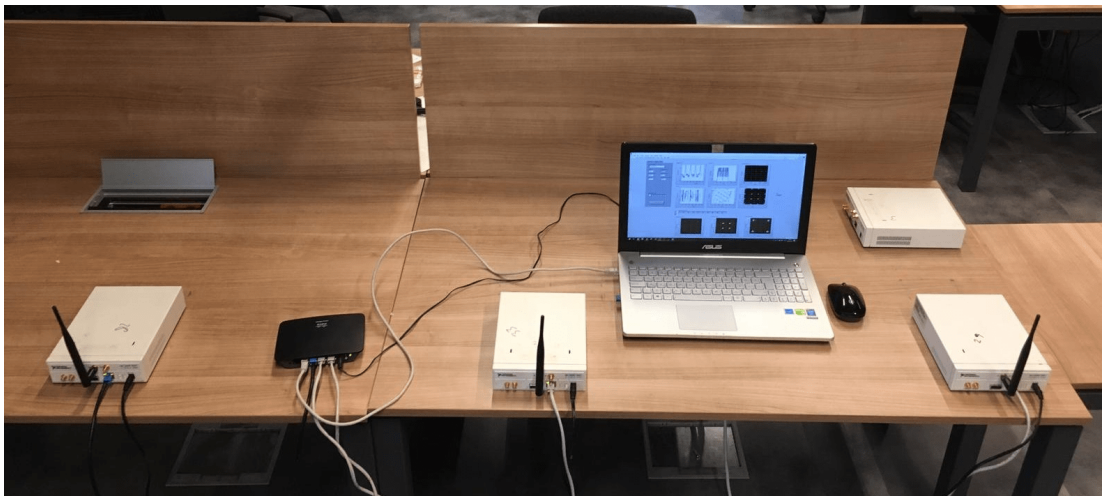

Figure 3.3 : Proposed test-bed.

LabVIEW, a visual programming language, was used as a software on the host computer to which USRP nodes are connected. During the design of the system, different communication blocks and signal processing blocks available in LabVIEW environment were utilized. In LabVIEW, the design of the orthogonal frequency division multiplexing (OFDM) receiver and transmitter designs are integrated by the NOMA system components. The parameter values used during the tests are shown in Table 3.1.

In the tests performed, the data bits were first converted to 4-QAM symbols in the source side. After multiplying the power allocation coefficients, the different data symbols of the two users are superimposed. The power of the frequency spectrum of NOMA and OMA systems has been kept constant in terms of a fair system design. The power allocation coefficient of the UE_1 was determined as $\alpha = 0.2$, and therefore the power allocation coefficient of the UE_2 was determined as $\alpha = 0.8$. After the allocation is operated and symbols are combined, the new symbols obtained are converted into OFDM signal. To do this, first of all the pilot symbols are added to the new symbols. Finally, the cyclic prefix (CP) is added to the transmit signal.

Users first apply OFDM demodulation to the signals received. After synchronization, the CP part is removed from the signal and the signal is passed to the frequency axis with the fast Fourier transform (FFT). In the transmitter, channel estimation is performed with the help of pilot signals added to the signals. After this step, the signal of the UE_2 is converted to message bits by the QAM demodulator. The UE_1 obtains

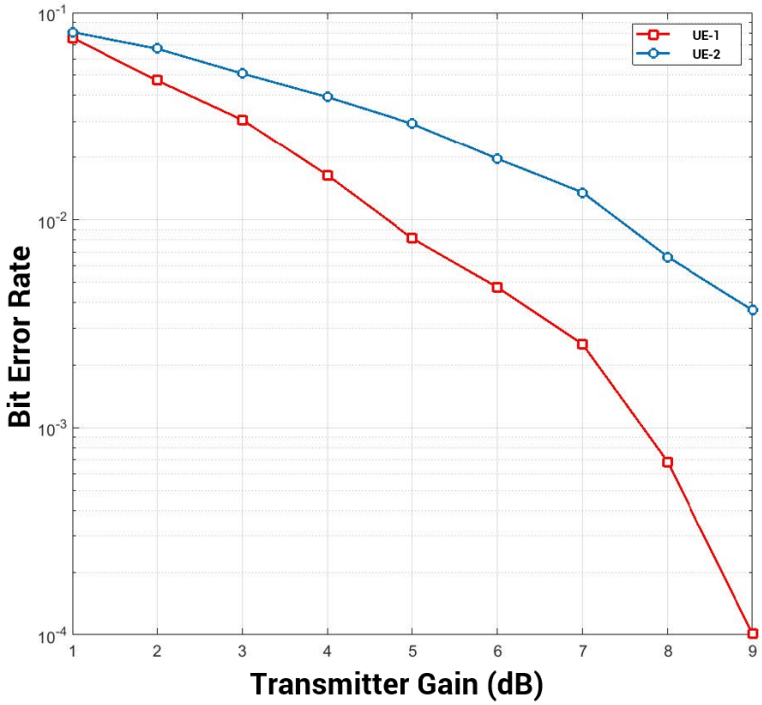

Figure 3.4 : The bit error rates of the users according to the transmitter gain.

the signal by removing the signalof the UE_2 with the SIC before converting the signal to the message bits. Here, it is assumed that the UE_1 knows the power allocation coefficients determined by the transmitter.

3.4 Results

In this section, real-time average bit error rate (BER) measurements for analyzing users' performance are given in detail. In the first scenario, the distance between the UE_1 and the source is 1 meter and the distance between UE_2 and the source is 2 meters. 1250 $bits/symbol$ is generated for each user in the source. An average of 800 NOMA-OFDM symbols were transmitted in each test and the tests were repeated 10 times. As a result of the tests, the effect of different transmitter gain applications on the bit error rate of the signals received by the users is shown in Figure 3.4. While the BER value of UE_1 is 7×10^{-2} with 1 dB transmitter gain at the source, the BER value decreases to 1×10^{-4} when the transmitter gain is increased to 9 dB. The BER value of UE_2 is 8×10^{-2} for the 1 dB transmitter gain and 3×10^{-3} for 9 dB transmitter gain. Also, when compared to users in terms of BER values, it is observed that the close user provides better performance for each gain value.

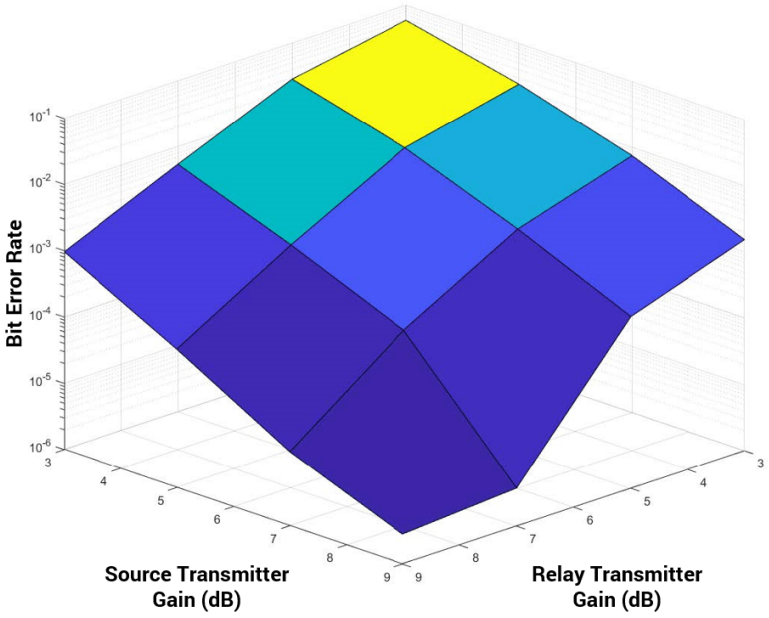

Figure 3.5 : The bit error rates of UE-1.

In the second scenario, the transmission between the source and the users is provided with the help of a relay. In these tests, the relay is placed 1 meter away from the source, 1 meter away from the $UE-1$ and 2 meters from the UE_2. Here, the communication between the source and the relay is communicated at different frequencies so that there is no direct connection between the source and the users. The error performance for UE_1 is given in Figure 3.5 and for UE_2 in Figure 3.6. Measurements were repeated with different transmitter gains on both the source and relay nodes. This shows the effect of the power factor on the relay.

The results of these tests compared to the values in Figure 3.4, although the distance from users to the source is higher than the first scenario, performance loss was not experienced in tests with high relay gain. In the relay system for the same source transmitter gain, the BER values in the high relay gain for UE_1 have been reduced and the BER values are approximately preserved for UE_2.

By examining the values in these tests, the most appropriate transmitter gain to be used in the relay can be determined. For example, while the relay gain was 5 dB, BER values on the first scenario and the second scenario for UE_1 were found to be close to each other.

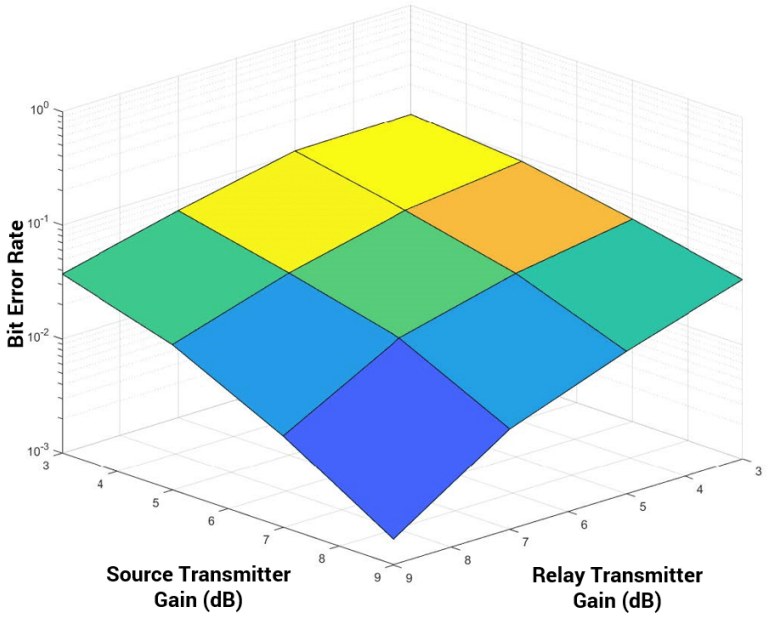

Figure 3.6 : The bit error rates of UE-2.

These BER values for 3 dB source transmitter gain are 2.8×10^{-2} and 3×10^{-2} with relay and without relay, respectively. These BER values for 7 dB source transmitter gain are 2.1×10^{-3} and 2.5×10^{-3} with relay and without relay, respectively.

Similarly, when two scenarios are compared for UE_2, it is seen that with relay and without relay systems give close results under 7 dB relay gain. These BER values for 3 dB source transmitter gain are 6×10^{-2} and 5×10^{-2} with relay and without relay, respectively. These BER values for 7 dB source transmitter gain are 2×10^{-2} and 1.3×10^{-2} with relay and without relay, respectively.

3.5 Conclusion

In this study, an experimental platform consisting of USRP nodes was used to construct a real-time test system. An OFDM-based downlink NOMA system that can be used to verify and evaluate the performance of numerous approaches to NOMA, which in theory increases SE of wireless networks in particular, has been established. In this system, SC and SIC algorithms are investigated on the power domain NOMA system. As a result of real-time tests carried out in the laboratory without relay and with relay, bit error rates of the users have been obtained. The performance of NOMA is shown in a real-time test environment, outside the simulation environment.

4. UF-OFDM

4.1 Introduction

Mobile communications constitute an indispensable component of our daily lives. The development of Long Term Evolution (LTE) technology has provided significant improvements in spectral efficiency and data rates, addressing user demands. However, the ease of use and the day-to-day development of more skillful communication technologies are leading to an increase both in the usage frequencies and in the user expectations. This demand is further triggered of the boost of applications like Internet of Things (IoT) networks. To meet the stringent requirements of future expectations, the search for new technologies is a must. Although traditional cyclic prefix orthogonal frequency division multiplexing (CP-OFDM), a waveform which constitutes the main component of LTE systems, is a crucial part of 5G networks, researchers propose various signaling schemes addressing user demands, as described in [13], to alleviate implementation problems associated with CP-OFDM. Major problems of the CP-OFDM technique include tight synchronization requirements, reduced spectral efficiency of cyclic prefix and high spectral out-of-band (OoB) emissions.

High OoB emissions cause interference between adjacent channels [14] and spectral efficiency is negatively affected. The main technique for preventing adjacent channel interference (ACI), observed due to non-zero OoB emissions, is to place guard bands between adjacent CP-OFDM symbols [15], thereby to reduce the OoB effects. The guard band, which cannot be used for data transmission, presents a loss in terms of spectral efficiency. As another method, when generating an CP-OFDM symbol, unused subcarriers are utilized and OoB emissions are reduced [16]. This method also reduces the spectral efficiency due to unnecessary use of subcarriers. Apart from these general applications, there are different OoB energy reduction methods in the literature, as cancellation carriers placed on both sides of the CP-OFDM symbol [17], subcarrier weighting [18] or using of multiple choice sequences [19] that reduce OoB

emissions. The most significant effect of these methods is to reduce the spectral efficiency and to cause additional signaling overhead. As a more recent method, the filtering of the CP-OFDM symbol leads to serious reductions in OoB emissions, in addition to the resistance to interference [20]. However, the filtering process increases complexity and causes latency in the transmitter and the receiver [21].

As a proposed waveform to address CP-OFDM's inefficiencies, universal filtered orthogonal frequency division multiplexing (UF-OFDM), also known as universal filtered multi carrier (UFMC), emerges a serious waveform candidate for future generation cellular systems in order to solve some problems like OoB emissions of the CP-OFDM technique with the use of filtering. In the UF-OFDM technique, filtering process is applied to the blocks of narrow band subcarriers, called sub-bands [**?**]. This results in an increase in the spectral efficiency, while providing protection against interference between symbols. Synchronization of UF-OFDM is simpler than that of CP-OFDM [22]. Furthermore, UF-OFDM has similar signal processing steps to CP-OFDM. Most of the proposed methods for CP-OFDM also apply to UF-OFDM. According to [22], UF-OFDM is a well-suited technique for short burst transmissions and enabling low latency modes.

The intensive performance of expectation of beyond 5G networks requires to make efficient use of the frequency band. Unfortunately, when CP-OFDM is used, it is necessary to leave a guard band in the spectrum to eliminate ACI from side lobes. This reduces the spectral efficiency and hence poses a problem to meet design goals. Suppressed side lobes of UF-OFDM can alleviate this problem and the overall spectral efficiency can be increased with the use of UF-OFDM.

In this paper, we compare the performances of UF-OFDM and CP-OFDM in presence of ACI, though real-time tests based on the designed and implemented test platform. Real-time power spectra of CP-OFDM and UF-OFDM are shown in Figure 4.1, varying according to different transmitter (TX) gain values. Accordingly, it is observed that CP-OFDM has higher OoB emissions than that of UF-OFDM. As the most prominent problem in real-time systems, synchronization problems have been addressed in the tests and an appropriate and fair comparison environment has been created. Carrier frequency offset (CFO) and the sample timing offset (STO) estimation methods described in [23] are applied. The comparison environment is

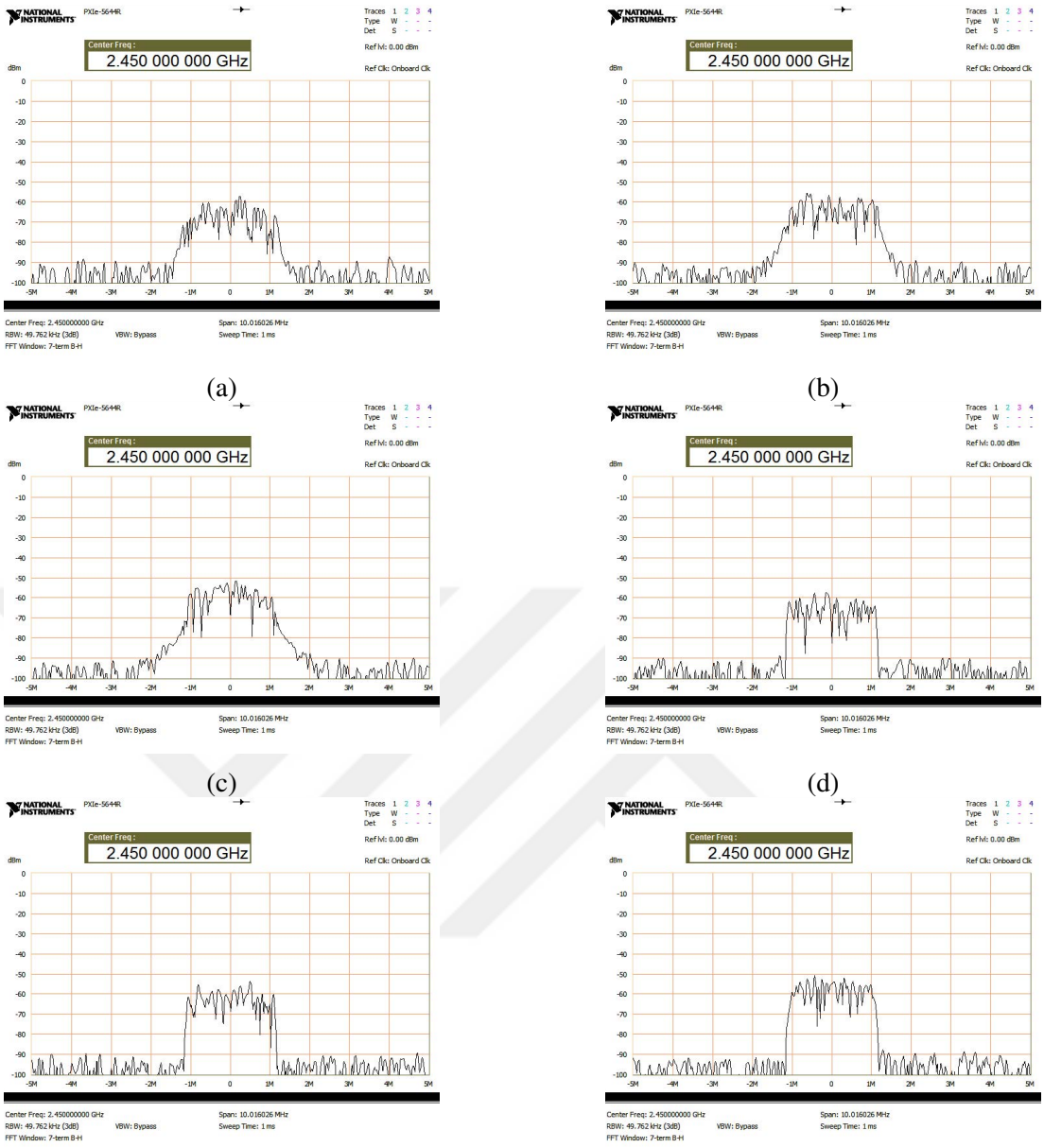

(a) (b)

(c) (d)

(e) (f)

Figure 4.1 : Frequency spectra. (a) CP-OFDM 5dB TX gain. (b) CP-OFDM 10dB TX gain. (c) CP-OFDM 15dB TX gain. (d) UF-OFDM 5dB TX gain. (e) UF-OFDM 10dB TX gain. (e) UF-OFDM 15dB TX gain.

designed as both Single Input - Single Output (SISO) and Single Input - Multiple Output (SIMO) configurations. Maximal-Ratio Combining (MRC), as detailed in [24], is used in SIMO system. The comb-type least square (LS) method of channel estimation technique has been used to remove the channel effects. In addition to this, the CP-OFDM technique is also examined in the same system, and fair performance comparisons are made. USRP-2943R and USRP-2921 software defined radio (SDR) nodes are used as transmitter, receiver and interfering transmitters and the application has been developed using LABVIEW. UF-OFDM and CP-OFDM comparisons are

presented using signal-to-noise ratio (SNR), bit error rate (BER), symbol error rate (SER) and error vector magnitude (EVM) metrics. The impact of the guard-bands on the error performances between different adjacent channels are also highlighted.

4.2 Related Works

In order to overcome the shortcomings of CP-OFDM, various different waveform solutions have been proposed in the literature. The most frequently discussed waveforms with filtering include, generalized frequency division multiplexing (GFDM), filter bank multicarrier (FBMC), UF-OFDM and filtered OFDM (F-OFDM), that aim to improve the performance of CP-OFDM.

In FBMC, frequency domain filtering is performed at the subcarrier level to obtain lower OoB emissions and a higher spectral efficiency than CP-OFDM [25]. Overlapping is applied to the FBMC, which does not include CP requirements, and the resulting inter symbol interference (ISI) is eliminated by using offset-quadrature amplitude modulation (OQAM) [26]. However, the use of OQAM worsens the multiple input multiple output (MIMO) performance. In addition, peak-to-average power ratio (PAPR) of FBMC is lower than CP-OFDM [27].

GFDM, which has a complicated transmitter and receiver structure than FBMC, uses a multi-dimensional block structure with CP and cyclic shift (CS) is performed with every filter used [28]. Frequency and time domain multi-user scheduling can be performed and the bandwidth of the blocks can be changed by using GFDM [29]. According to FBMC, GFDM has a worse spectral efficiency and higher OoB emissions [30]. According to FBMC, GFDM has a poor performance and higher OoB emissions [31]. However, with the linear GFDM structure in [32], OoB emissions can be reduced to the FBMC level. GFDM is also more successful than FBMC in terms of MIMO compatibility. Additionally PAPR of GFDM is much lower than that of CP-OFDM [31].

F-OFDM, which applies subband filtering such as UF-OFDM, offers different parameter approaches such as CP length and time transmission interval (TTI) for each subband than UF-OFDM [33]. Thus, different users and applications can become more harmonized. CP is used in F-OFDM. When compared to UF-OFDM and FBMC,

GFDM and F-OFDM are more flexible techniques [34]. As in the cases of GFDM and UF-OFDM, F-OFDM provides advantages in terms of MIMO compatibility [35].

The compatibility and improvement of these waveforms, which reduce the OoB emissions from the fundamental problems of CP-OFDM, in terms of different scenarios are still research topics. Various works have been carried out under different headings related to UF-OFDM, which comes in the forefront from filter usage based waveforms.

UF-OFDM is less complex than FBMC, and its use seems more practical since it can provide a similar performance. UF-OFDM is a more convenient option for beyond 5G applications due to its lower latency than GFDM and FBMC [36]. It is also a good candidate for massive MIMO applications. However, the complex orthogonality of the subbands is lost, albeit very little, due to the summation process [37]. In addition to ensuring spectral efficiency due to the absence of CP, multi-tap equalizers are required for multi-path cases and thus the associated complexity is increased [38].

From the implementation aspects, CFO is a fundamental problem that results from Doppler shift and synchronization problems between transmitter and receiver oscillators and it affects communication performance negatively [39]. In order to eliminate the CFO effect, CFO estimation and correction processes must be performed at the receiver. Simpler and more easily implemented CFO estimation techniques in single carrier systems are becoming more complicated and more important because of the inter carrier interference (ICI) caused by CFO in multicarrier systems [40].

In real-time applications, CFO is an inevitable reality and there are quite different approaches as time domain and frequency domain CFO estimation techniques in the literature to overcome its destructive effects. OoB emissions is also one of the reasons that may contribute to the effect of CFO. In particular, power components of OoB emissions of the signal make it difficult to estimate the CFO correctly and worsen the error performance of the correction algorithms. Applications like filtering approaches, that increase the resistance of the CFO effect to the signal in the performance of the CFO estimation techniques, are also of interest [41]. For this reason, waveform options such as UF-OFDM are recommended for beyond 5G systems to reduce the CFO effect and increase the estimation and correction performance.

Apart from the benefits of CFO on the filter use, there is also a complexity enhancing effect. The complexity of inverse discrete Fourier transform (IDFT), finite impulse response (FIR) filter, and spectrum shifting blocks of a UF-OFDM transmitter structures is reduced by different methods as in [42] on UF-OFDM. With UF-OFDM, which is more resistant than CP-OFDM, the use of low-cost oscillators is feasible even in presence of the CFO effect. However, CFO estimation techniques have to be adapted to UF-OFDM. The hybrid CFO estimation scheme presented in [43] can achieve a larger estimation range and a higher estimation precision than conventional CFO estimation techniques.

In terms of the design issues, there are different approaches in the literature for filter selection and development processes. The adaptive filter configuration algorithm proposed in [44] dramatically eliminates the interference caused by different CFOs, and achieves a better BER performance and a higher rate than the conventional scheme. Instead of the Dolph-Chebyshev filter used in conventional systems, a scheme that is more controllable and offers a higher BER performance, as shown in [45].

In the receiver structure used in the conventional UF-OFDM system presented in [46], odd subcarriers are not utilized. A receiver scheme using odd subcarriers, presented in [47], performs better on both additive white Gaussian noise (AWGN) and frequency selective channels. However, it is observed that the proposed receiver structure is more resistant to frequency synchronization errors.

Despite the fact that a large number of computer simulations have been conducted; UF-OFDM, as a real-time application, has been subject to research only up to daylight, only in [**?**]. In this study, UF-OFDM and CP-OFDM systems were evaluated in terms of EVM and BER values to determine OoB emission effect. In this work, we provide more insights about the performance of UF-OFDM in presence of ACI through the designed and implemented test-bed, as detailed below.

By separating the available bandwidth into multiple independent narrowband subcarriers that use a much smaller bandwidth than the entire band, multicarrier techniques offer high spectral efficiency and high data rate promises [48]. Moreover, more successful communication can be achieved even in the presence of the frequency selective channels since subcarriers have a much smaller bandwidth. Below we provide

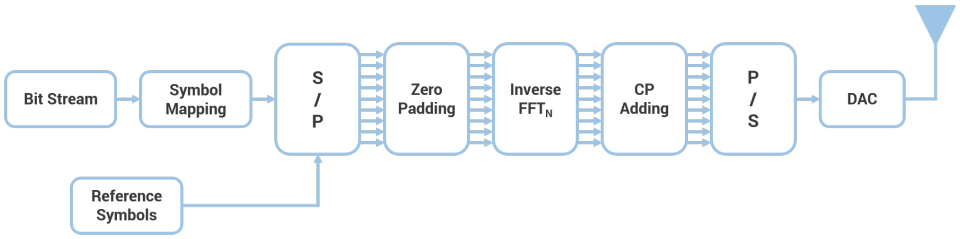

(a)

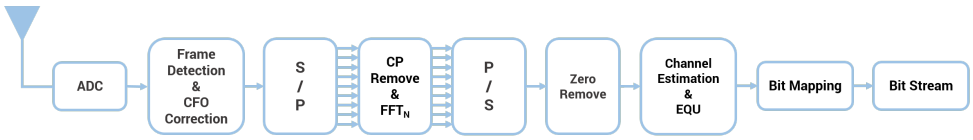

(b)

Figure 4.2 : Block diagram of CP-OFDM. (a) Transmitter. (b) Receiver.

the system models for CP-OFDM and UF-OFDM in SISO. Unlike SISO, in the SIMO system, the channel information is obtained in the receiver up to the number of RF chains. Therefore, MRC is used in the receiver as described in [24]. We follow the notation in [46]. In formula notations, lowercase letters are used in the time domain representations and uppercase letters are used in the frequency domain representations during the article. $(\cdot)^T$ and $(\cdot)^H$ refer to transpose and conjugate transpose, respectively. $\mathscr{C}$ symbolizes the set of complex-valued numbers and $\mathscr{R}$ indicates the set of real-valued numbers. $\text{diag}\{a_1, a_2, \cdots, a_n\}$ and I_N represent the diagonal matrix of $n \times n$ and identity matrix of $N \times N$, respectively.

4.3 CP-OFDM

As detailed in [49], CP-OFDM uses IFFT to construct orthogonal subcarriers. The signal consisting of the reference and data symbols transformed to the time domain is transmitted by appending CP. In the receiver, firstly the CFO and STO correction from the channel is made. Using FFT, the transmitted signal is fed back. Finally, channel estimation is performed by using reference symbols for equalization. Figure 4.2(a) and 4.2(b) show the CP-OFDM transmitter and receiver structures, respectively.

Let N denote the number of subcarriers. The CP length is denoted by N_{CP}. The CP which is added to each OFDM symbol to eliminate ISI effects. Each OFDM symbol's

block length is $N_B = N_{CP} + N$. The channel between the receiver and the transmitter is fixed during the OFDM symbol period under the assumption that channel is the frequency-selective L-paths. The discrete-time received CP-OFDM symbol in CFO and in presence of ACI of K users (i.e. with a total of $K+1$ users) can be modeled as follows:

$$\mathbf{y} = \Omega_r \mathbf{h} \Gamma(\varepsilon) \Omega_t \mathbf{V}^H \mathbf{X} + \mathbf{w} + \mathbf{z}(\Psi, K), \tag{4.1}$$

where

$$\mathbf{X} = [X(0),\ X(1),\ \cdots,\ X(N-1)]^T, \tag{4.2}$$

is the transmitted symbol sequence,

$$\Omega_t = [[0\ \mathbf{I}_{N_{CP}}]\mathbf{I}_N], \tag{4.3}$$

represents the CP insertion matrix,

$$\Gamma(\varepsilon) = \text{diag}\left\{1,\ e^{\frac{2\pi\varepsilon}{N}},\ \ldots\ e^{\frac{2\pi(N-1)\varepsilon}{N}}\right\}, \tag{4.4}$$

represents the CFO matrix, where $\varepsilon = \frac{f}{\triangle f} = \frac{f}{f_t - f_r}$ is the normalized frequency. f_t and f_r are carrier frequency at the transmitter and the receiver, respectively. The CP removal matrix is denoted by

$$\Omega_r = [0\ \mathbf{I}_N]. \tag{4.5}$$

The channel vector is denoted by $\mathbf{h}$, whose first column is $[h(0),\ h(1),\ \cdots,\ h(L-1),\ 0,\ \cdots,\ 0]^T$ defines the Toeplitz channel matrix with channel gain $h(l)$. $\mathbf{w}$ denotes the independent identically distributed (i.i.d.) complex Gaussian random variables denotes the AWGN on channel and $\mathbf{z}(\Psi, k)$ represents the ACI component and the guard band between CP-OFDM signals are denoted by Ψ. Note that

$$\mathbf{z}(\Psi, K) = \sum_{k=1}^{K} \alpha_{CP}(\Psi, k) \Omega_r \mathbf{h}^k \Gamma(\varepsilon^k) \Omega_t \mathbf{V}^H \mathbf{X}_k, \tag{4.6}$$

where $\mathbf{h}^k$ is the channel between the k-th user and the target receiver. $\Gamma(\varepsilon^k)$ and $\mathbf{X}_k$ represents the CFO matrix and the transmitted signal corresponding to the k-th user. The ACI coefficient, $\alpha_{CP}(\Psi,k) = 0$ in the absence of OoB emissions, however due to non-zero OoB be observe $\alpha_{CP}(\Psi,k) << 1$, whose value depends on the signaling model.

The received signal in frequency-domain, can be stated as

$$\mathbf{Y} = \mathbf{HQX} + \mathbf{W} + \mathbf{Z}, \tag{4.7}$$

where

$$\mathbf{Y} = [Y(0),\, Y(1),\, \cdots,\, Y(N-1)]^T, \tag{4.8}$$

and

$$\mathbf{H} = \text{diag}\{H(0),\, H(1),\, \cdots, H(N-1)\}. \tag{4.9}$$

In equation (7), $\mathbf{Q}$ is defined as

$$\mathbf{Q} = \mathbf{V}\Gamma(\varepsilon)\mathbf{V}^H, \tag{4.10}$$

and

$$\mathbf{Q} = \begin{bmatrix} q(0) & q(1) & \dots & q(N-1) \\ q(-1) & q(0) & \dots & q(N-2) \\ \vdots & \vdots & \ddots & \vdots \\ q(-N+1) & q(-N+2) & \dots & q(0) \end{bmatrix}, \tag{4.11}$$

where

$$q(n) = \frac{1}{N} \sum_{q=0}^{N-1} \exp\left(\frac{j2\pi q(\varepsilon + n)}{N}\right). \tag{4.12}$$

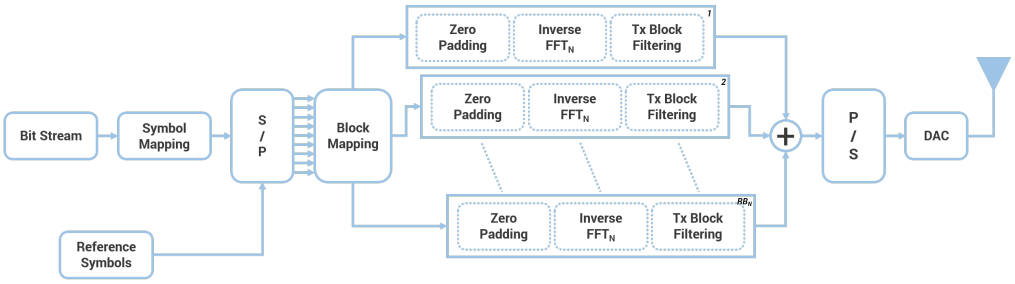

Figure 4.3 : UF-OFDM transmitter.

4.4 UF-OFDM

Since UF-OFDM transmitter and receiver uses matrix multiplexing and includes filtering, it is relatively more complex than CP-OFDM receiver and transmitter structure [46]. The complexity of UF-OFDM can be reasonably afforded because of the more successful transmission. UF-OFDM, has a similar PAPR performance as CP-OFDM. However its PAPR value can reduced by using different algorithms as in [50], but this increases the complexity.

UF-OFDM is based on the filtering of blocks consisting of at least two subcarriers to reduce the power spectral density (PSD) of the OoB emissions [51]. The filtering approach is also valid for the FBMC. Each subcarrier is filtered in the FBMC and thus it is highly resistant to ICI [52]. However, the filtering operation of each subcarrier increases complexity and the desired short burst time value for 5G [22] and beyond 5G. This makes it difficult to realize an energy efficient communication system. The UF-OFDM which is much closer to CP-OFDM than FBMC is a much more affordable version of the FBMC technique. The most important difference from CP-OFDM is that there is no CP obligation in UF-OFDM. The block diagram of the UF-OFDM transmitter is shown in Figure 4.3.

The symbol components of QAM, used as the modulation technique, are generated from the data bits belonging to the users. Pilot symbols used to obtain channel information can be placed between the data bits at the desired frequency. The increase in the number of pilots reduces the spectral efficiency despite the increase in channel estimation performance.

The obtained UF-OFDM symbols are divided into N_{RB} blocks which have $\widetilde{N} = \frac{N}{N_{RB}}$ data symbols for one block and each block is subjected to IFFT and filtering operations respectively. Signals formed after filtration are collected in the time domain and transmitted through the channel.

The time domain transmitted signal in UF-OFDM system can be expressed as

$$\mathbf{x} = \widetilde{\mathbf{F}}^H \widetilde{\mathbf{V}}^H \mathbf{X}, \tag{4.13}$$

where

$$\mathbf{X} = \left[\mathbf{X}_1^T,\, \mathbf{X}_2^T,\, \cdots,\, \mathbf{X}_{N_{RB}}^T\right]^T \in \mathscr{C}^{N\times 1}, \tag{4.14}$$

and

$$\mathbf{X}_p = \left[X_p(0),\, X_p(1),\, \cdots,\, X_p(\tilde{N}-1)\right]^T. \tag{4.15}$$

$\mathbf{V}$ is defined as

$$\widetilde{\mathbf{V}}^H = \mathrm{diag}\left\{\mathbf{V}_1,\, \mathbf{V}_2,\, \cdots,\, \mathbf{V}_{N_{RB}}\right\}, \tag{4.16}$$

and

$$\widetilde{\mathbf{F}}^H = \left[\mathbf{F}_1,\, \mathbf{F}_2,\, \cdots,\, \mathbf{F}_{N_{RB}}\right]. \tag{4.17}$$

In equation 4.13, $\mathbf{x}$, $\widetilde{\mathbf{F}}$, $\widetilde{\mathbf{V}}$ and $\mathbf{X} \in \mathscr{C}^{N\times 1}$ represent the transmitted UF-OFDM symbol, FIR filter matrix, Fourier matrix and data stream, respectively. $\mathbf{X}_p$ is the data stream of p-th sub-band. In (16), $\mathbf{V}_p \in \mathscr{C}^{N\times\tilde{N}}$ consists of $\tilde{N}$ columns of $\mathbf{V}$, starting from column $(p-1)\tilde{N}+1$. Filter matrix's entry $\mathbf{F}_p$ is the Toeplitz matrix whose first column is $[b_p(0),\, b_p(1),\, \cdots,\, b_p(L_{FIR}-1),\, 0,\, \cdots,\, 0]^T$. The coefficients $b_p(j)$ for $j \in \{0,1,\cdots,L_{FIR}-1\}$ are the p-th resource block FIR filter coefficients. Moreover, per-block filter coefficients are normalized as $\sum_{j=0}^{L_{FIR}-1} |b_p(j)|^2 = 1$.

With the linear convolution process used for filtration, $N + L_{FIR} - 1$ samples are obtained for each filtered sub-band. The goal of FIR filtering is to reduce OoB

emission values resulting from high side lobes of CP-OFDM. The maximum OoB radiation value can be reduced with the Dolph-Chebyshev FIR filter [53]. High OoB radiation values disturb the orthogonality between adjacent subcarriers, leading to synchronization errors and sensitivity [54]. As shown in Figure 4.1, OoB radiation levels are significantly reduced with the UF-OFDM compared to CP-OFDM. As a result, synchronization is more flexible; especially when there is less interference between sub-bands and orthogonality is preserved.

The time domain received signal and the frequency domain received signal in UF-OFDM system can respectively be expressed as

$$\mathbf{y} = \mathbf{h}\Gamma(\varepsilon)\widetilde{\mathbf{F}}^H\widetilde{\mathbf{V}}^H\mathbf{X} + \mathbf{w} + \mathbf{z}(\Psi, K), \tag{4.18}$$

where

$$\mathbf{Y} = \mathbf{H}\widetilde{\mathbf{Q}}\mathbf{X} + \mathbf{W} + \mathbf{Z}, \tag{4.19}$$

and the matrix $\widetilde{\mathbf{Q}}$ can be expressed as

$$\widetilde{\mathbf{Q}} = \widetilde{\mathbf{V}}\widetilde{\mathbf{F}}\Gamma(\varepsilon)\widetilde{\mathbf{F}}^H\widetilde{\mathbf{V}}^H. \tag{4.20}$$

ACI can be modeled in UF-OFDM with ACI coefficient $\alpha_{UF}(\Psi, k)$

$$\mathbf{z}(\Psi, K) = \sum_{k=1}^{K} \alpha_{UF}(\Psi, k)\Omega_r\mathbf{h}^k\Gamma(\varepsilon^k)\Omega_t\widetilde{\mathbf{V}}^H\mathbf{X}_k. \tag{4.21}$$

Filter equalization is required to remove distortions caused by filtering. Although there are different equalization methods for UF-OFDM systems, this work uses the often preferred zero-forcing (ZF) equalizer. To do so, the received signal vector is multiplied with $\mathbf{G}_{ZF}$ that is a equalization matrix that can be computed as

$$\mathbf{G}_{ZF} = (\mathbf{H}_{eff}^H\mathbf{H}_{eff})^{-1}\mathbf{H}_{eff}^H, \tag{4.22}$$

where $\mathbf{H}_{eff} = \mathbf{H}\widetilde{\mathbf{Q}}$ for UF-OFDM and $\mathbf{H}_{eff} = \mathbf{H}\mathbf{Q}$ for CP-OFDM systems. Figure 4.4 shows the UF-OFDM receiver structure.

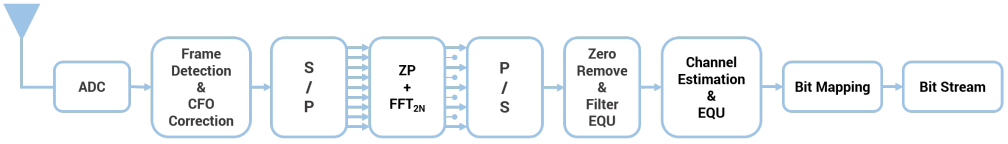

Figure 4.4 : UF-OFDM receiver.

The even indices from the symbols of the 2N point FFT result only include UF-OFDM samples, while the odd indexes contain interference. Odd indexed symbols are not used. Thus, by taking samples that are not interrupted between symbols, the sequence length to be processed is equal to N. AWGN in the channel, the result of 2N point FFT processing, is transformed into related colored noise among the different subcarriers. This ensures that the noise component is more effective.

In the pilot-based channel estimation, UF-OFDM (also in CP-OFDM) channel estimation symbols are periodically transmitted using all subcarriers. The aim is to estimate the channel condition, i.e. channel coefficients, with the aid of known pilot symbols. At the receiver these coefficients are generalized by linear interpolation until the next plot symbol and the received signal is corrected according to the channel estimation. In this study, we use least square method for channel estimation. The least squares method provides estimates of parameters under two conditions, minimizing the quadratic discrepancies between the observed data and the pilot data [55]. It is a simple and effective method.

The lack of a CP does not completely eliminate inter symbol interference (ISI) which is the result of multipath effects. If the UF-OFDM is in a multi path channel, it is expected that the increase of the paths will cause an increase in ISI and ICI as a consequence of not using the CP. However, resistance to the delay spread in the channel is ensured as another consequence of the filtering process. As mentioned in [56], it is understood that ISI and ICI may be ignored if the delay spread length is sufficiently small compared to L. However, it is theoretically possible that ISI component can be completely eliminated in cases where the CP length is bigger than the channel paths in CP-OFDM [57]. OoB radiation reduced by filtration at UF-OFDM causes

reducing or removing the number of guard subcarriers (GS) which are imperative to use in CP-OFDM and reduces spectral efficiency between adjacent channels.

4.5 Proposed Test-bed

In the proposed test-bed, we use two USRP-2943R with two RF chains and one USRP-2921 with one RF chain as SDR nodes, programming through LabVIEW is a graphical programming language, which is often used to simulate and examine communication systems and work with traditional coding. LabVIEW makes use of Virtual Instruments (VI) that are composed of two components.The block diagram is the section where the actual operations are performed and the design is constructed. The front panel allows the management of the block diagram and the retrieval of the results [58].

Universal Software Radio Peripheral (USRP) is an SDR that is often preferred by research laboratories, offering a more cost-effective hardware platform than traditional SDR systems. USRP management is usually performed by the mainframe. Communication systems designed in base band can be tested in desired frequency band and bandwidth with up/down conversion with USRP. The USRP basically consists of a local oscillator, an FPGA from which digital signal processing operations are performed, analog to digital converters (ADC), digital to analog converters (DAC) and low pass filter subunits, modularly. This modularity allows the USRP to operate in DC and in a desired frequency band.

The USRP-2921 model with a maximum bandwidth of 24 MHz for 16-bit sample width and the USRP-2943R model with a maximum bandwidth of 40 MHz for 16-bit sample width used in this study operational in the industrial, scientific, and medical (ISM) band of 2.4 GHz to 2.5 GHz and 4.9 GHz to 5.9 GHz, which are frequently preferred in communication system tests. USRP nodes used as data transmitter and interference transmitter have output power from 17 dBm to 20 dBm and up to 35 dB of gain as a data transmitter as in [59] and up to 31.5 dB of gain as a interference transmitter and offers a maximum -15 dBm input power and 37.5 dB gain as a receiver detailed in [60]. USRP-2921 and USRP-2943R has a frequency accuracy (10 MHz reference without GPS antenna) of 2.5 ppm with using the temperature compensated crystal oscillator (TXCO). Thus, it is a suitable hardware option for waveform tests.

Real-time applications require some additional processed in order to solve problems caused by the channel and hardware impairments. In the receiver structure, the analog signal is transformed into a baseband signal, filtered and then sampled. The same local oscillator is used for down-conversion and sampling. The CFO is caused by asynchronous local oscillators of the transmitter and receiver and the Doppler shift [61]. CFO has negative consequences on signal quality and subcarriers, especially in multicarrier systems.

Timing and frequency offset estimation are the first processes applied to the sampled signal. In CP-OFDM (also in UF-OFDM) systems, pilot assisted structure and training symbols based estimation are used to minimize or possibly prevent performance degrading effects of CFO and STO [62]. In this study, Moose's method is used in frequency domain CFO estimation techniques. Moose has shown that CFO can be estimated by using training sequences in [63]. Repeating the same sequences are used for maximum likelihood estimate (MLE) of the CFO. The starting point of the symbols needs to be known so that Moose's algorithm can be used. In other words, STO estimation process must be performed before CFO estimation. In his paper, the MLE of the CFO is obtained as

$$\tilde{\varepsilon} = \frac{1}{2\pi}\tan^{-1}\{(\sum_{k=0}^{M-1}\mathrm{Im}[T_{2k}T_{1k}^{*}])(\sum_{k=0}^{M-1}\mathrm{Re}[T_{2k}T_{1k}^{*}])\}, \tag{4.23}$$

where $\tilde{\varepsilon}$, $\mathrm{Im}[\cdot]$, $\mathrm{Re}[\cdot]$, "*" and M is the CFO estimate, the imaginary part, the real part, complex conjugate and total number of training symbols, respectively. T_{1k} and T_{2k} are frequency domain representations of t_{1k} and t_{2k} consecutive training sequences. The working range of the method using two repetitive sequences is ± 0.5 as the normalized frequency. This range can be expanded by increasing the number of training sequences.

Training sequences are also used for STO estimation in the receiver [64]. The similarities in the same set of symbols are revealed by the help of autocorrelation process and the STO effect is eliminated by finding the value that minimizes the square difference of training sequences. STO is estimated as follows

$$\tilde{\delta} = \arg\min\left\{\frac{|\sum_{k=0}^{\frac{N}{2}-1} t_{1k}t_{2k}^{*}|^2}{|\sum_{k=0}^{\frac{N}{2}-1} t_{2k}|^2}\right\}. \tag{4.24}$$

Table 4.1 : Real-time test parameters.

FFT Size	256
Modulation	QAM
B_N / S_N	12 / 12
Filter / CP Length	40 / 39
Filter Sidelobe Magnitude	44 dB
d	50/100 cm
IQ Rate	2M
Carrier Frequency	2.45 GHz
Transmitter Gain	5/10/15 dB
Receiver Gain	0 dB
Data / Reference Symbols	120 / 24
Ψ	0/1.5/3/6 kHz
Receive Antenna	1 / 2

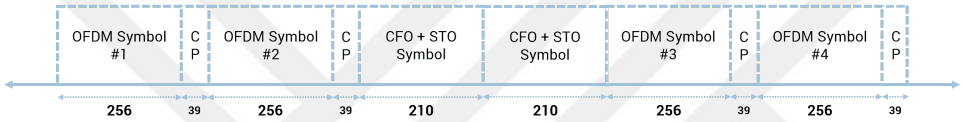

(a)

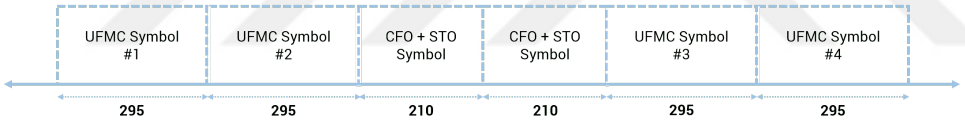

(b)

Figure 4.5 : Frame structures. (a) CP-OFDM. (b) UF-OFDM.

The frames of the CP-OFDM and UF-OFDM signals used in the tests are shown in the Figure 4.5(a) and 4.5(b), respectively. CFO and STO test symbols are placed in the middle of the frames for a better understanding of the ACI effect on boundary samples. Each frame consists of 1600 samples. In order to make a fair comparison, each CP-OFDM signal and UF-OFDM signal consists of equal number of samples. In a frame containing 4 different signals, there are a total of 480 data symbols and 96 reference symbols used for channel estimation. Unlike CP-OFDM, UF-OFDM does not have CPs. The training sequences, which are in the form of identical and framed signals, consist of 210 symbols. The parameters used in the real-time tests are given in the Table 1.

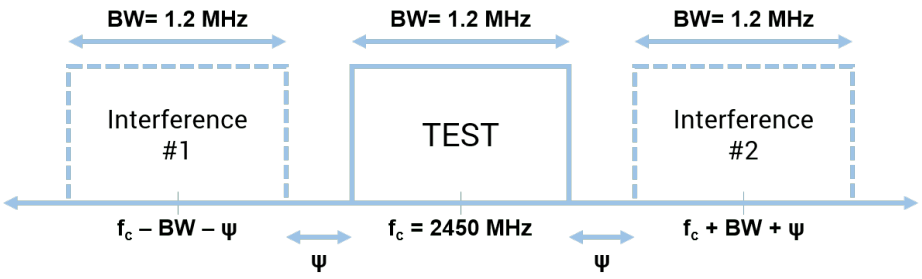

Figure 4.6 : Frequency band.

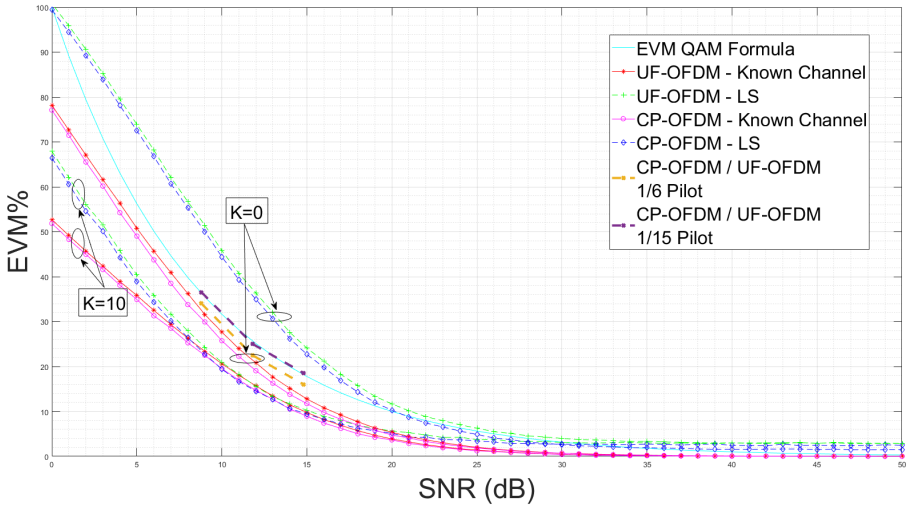

Figure 4.7 : Error vector magnitudes of CP-OFDM and UF-OFDM.

In the tests, two different interfere transmitters are used for ACI generation, except for receiver and transmitter. Tests were conducted at 2.45 GHz frequency band and 1.2 MHz bandwidth. The interference transmitters which consist of the waveform of the test transmitter are placed symmetrically to the used frequency band and at a distance of Ψ Hz. Ψ is varied to examine the interference effect during testing. The frequency bands of the test and interference devices are shown in the Figure 4.6.

EVM values provide information about the SNR. Even if the perfect SNR estimation can not be performed only with the EVM information, EVM-SNR conversion can be performed as described in [65]. The EVM to SNR equation for QAM, used in tests, is as follows

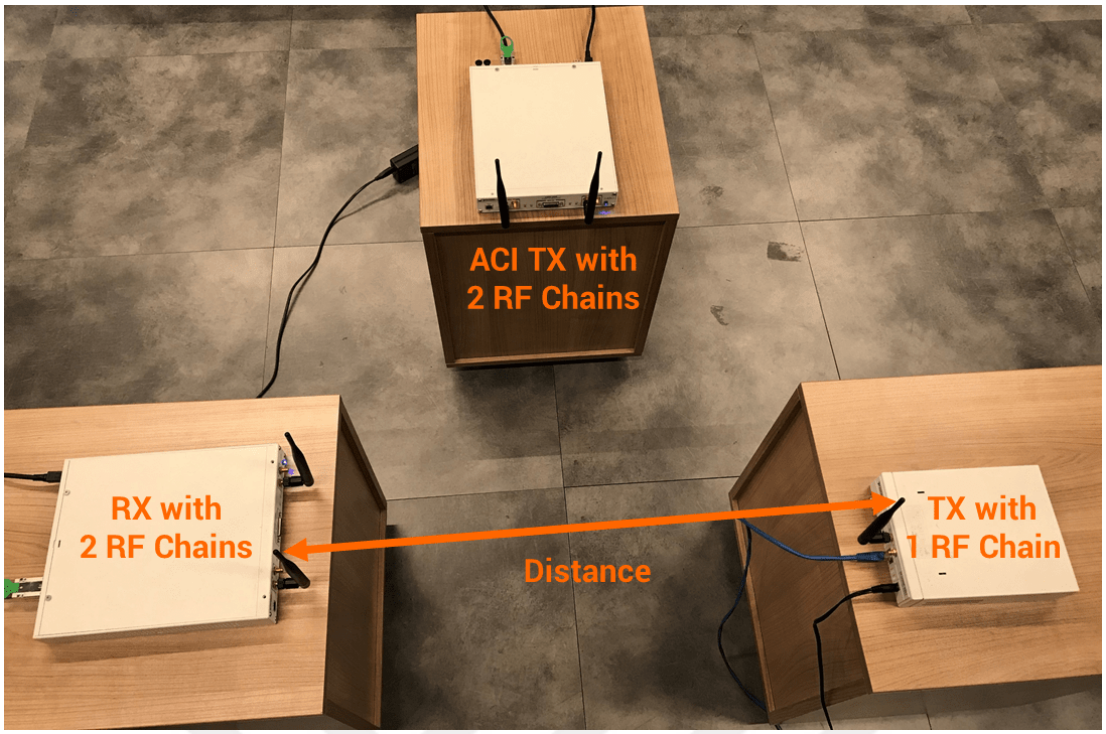

Figure 4.8 : Proposed test-bed.

$$EVM_{QAM} \cong \left[\frac{1}{SNR} - 4\sqrt{\frac{1}{2\pi SNR}} e^{-\frac{SNR}{2}} + 2 \ \text{erfc}\left(\sqrt{\frac{SNR}{2}} \right) \right]^{0.5} \tag{4.25}$$

Equation 4.25 is given in Figure 4.7. This formula gives approximately EVM value with simulations performed for SNR(dB)>25. Consequently, equation 4.25 for high SNR values can be evaluated as SNR estimation method. Real-time tests are performed on two USRP-2943R with two RF chains and one USRP-2921 with one RF chain using LabVIEW and PXI host. PXI provides power, cooling, and a communication bus for modular instruments or I/O modules that can be controlled these modules from either an embedded controller or an external PC, using one or several of specialized engineering software tools to customize the system. The timing module that enables a higher level of synchronization on the PXI platform through high-stability clocks, high-precision triggering and advanced signal routing for synchronization is used in test USRP nodes for clock. The proposed test-bed is shown in the Figure 4.8.

Simulations and real-time tests are carried out considering different parameters for performance comparison of CP-OFDM and UF-OFDM. During the real-time tests, the 4-Tap Rician Channel with $K = 10$ is observed as the approximate channel type. This

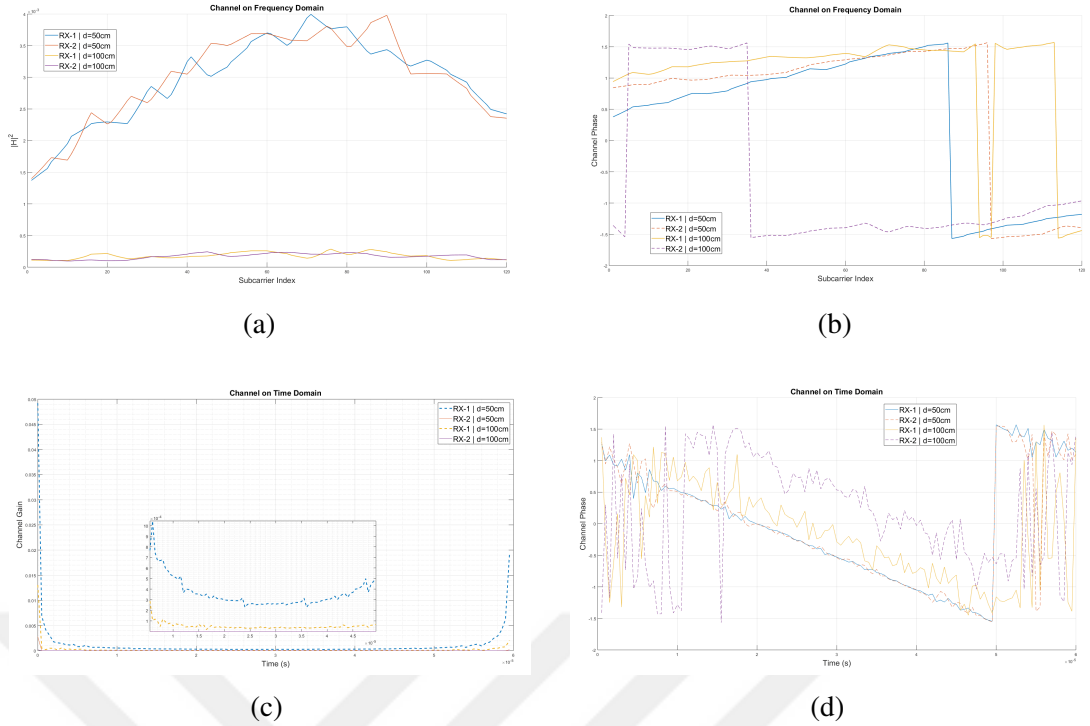

(a) (b)

(c) (d)

Figure 4.9 : Channel on the test environment. (a) Frequency domain - gain. (b) Frequency domain - phase. (c) Time domain - gain. (d) Time domain - phase.

channel is also used in simulations. The time and frequency domain representations of the channel of the test environment are shown in Figure 4.9.

The simulation results are shown in Figure 4.10 and Figure 4.11 under the assumption that channel information is known at the receiver correctly at 4-Tap Rician and Gaussian noisy channels with perfect synchronization.

In the simulation scenario where there is no CFO and STO, CP-OFDM is found to be more successful than UF-OFDM with about 1 dB SNR. In addition, the results of the EVM-SNR formula and the EVM values obtained in simulations based on the LS method used to obtain the channel information and the assumption that the actual channel information is known at the receiver are shown in the Figure 4.7 with different K values where K denotes the Rician channel parameter. As a result of the simulation, approximate values were obtained with the EVM formulation used. It is understood that good channel information is effective on EVM estimation. It is also seen that the LS method used is insufficient after a high SNR level and therefore causes an error-floor.

In real-time tests, it was observed that the frequency of the pilot symbol used for the channel information was also related to the EVM performance. In order to observe this

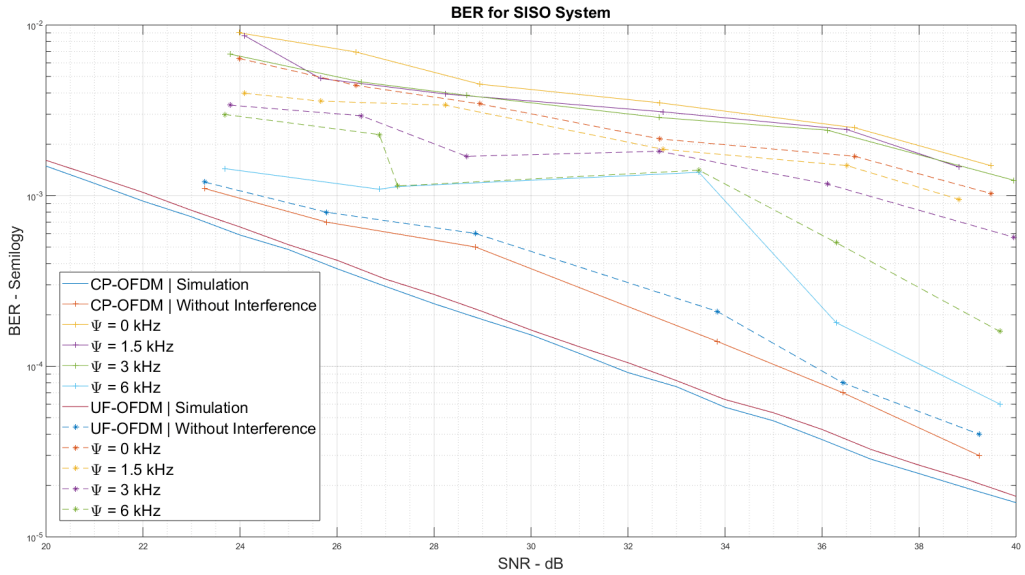

(a)

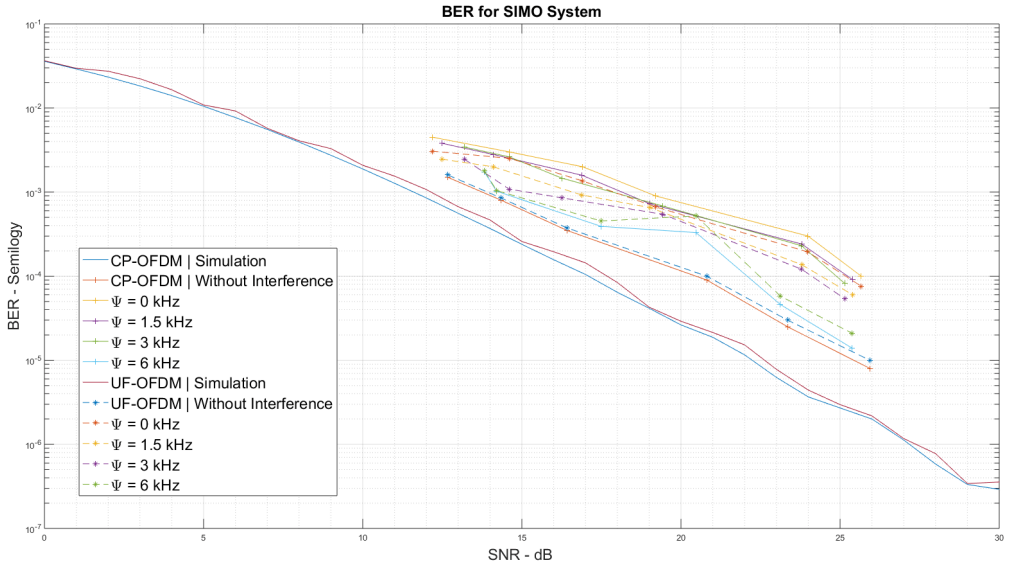

(b)

Figure 4.10 : Bit error rate vs SNR. (a) SISO system. (b) SIMO system.

relationship, in the tests without ACI, EVM values decreased as a result of the increase in pilot frequency. The results of the EVM obtained by the use of pilot symbols placed in 1/6 and 1/15 pilot frequencies are shown in Figure 4.7. This comparison was performed at 9-15 dB SNR levels because it was easier to observe the EVM difference for the low SNR level. It has been found that the CP-OFDM and UF-OFDM have approximately the same EVM values in low SNR values.

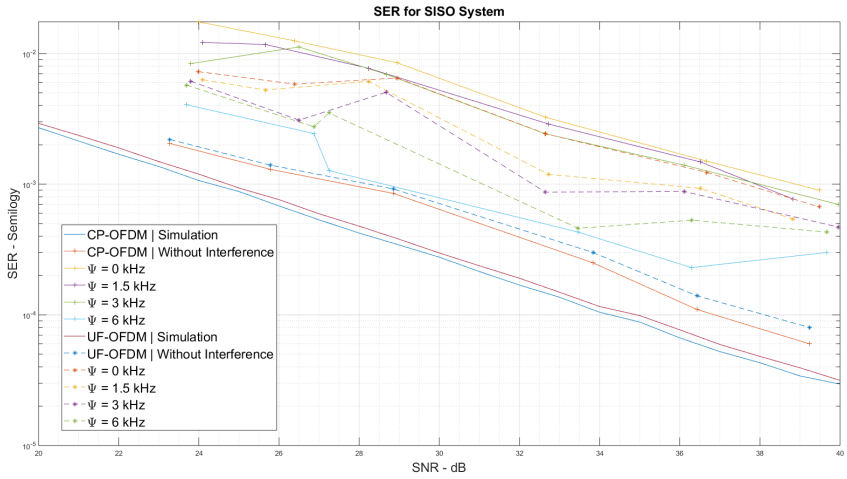

(a)

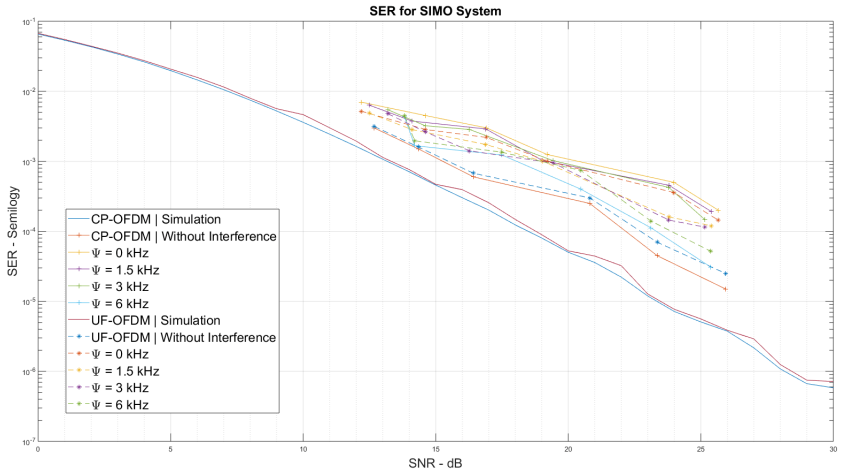

(b)

Figure 4.11 : Symbol error rate vs SNR. (a) SISO system. (b) SIMO system.

4.6 Results

Five different scenarios are applied in the real-time tests considering six different SNR levels to compare the performance of CP-OFDM and UF-OFDM on ACI because of OoB emissions. The results obtained are shown in Figure 4.10 and 4.11 for both SISO and SIMO system. In the first scenario, it is determined that CP-OFDM is more successful than UF-OFDM in terms of BER performance in the presence of near-perfect synchronization and no ACI generating transmitters. The same oscillator clock, STO and CTO estimation algorithms are evaluated for the synchronization process.

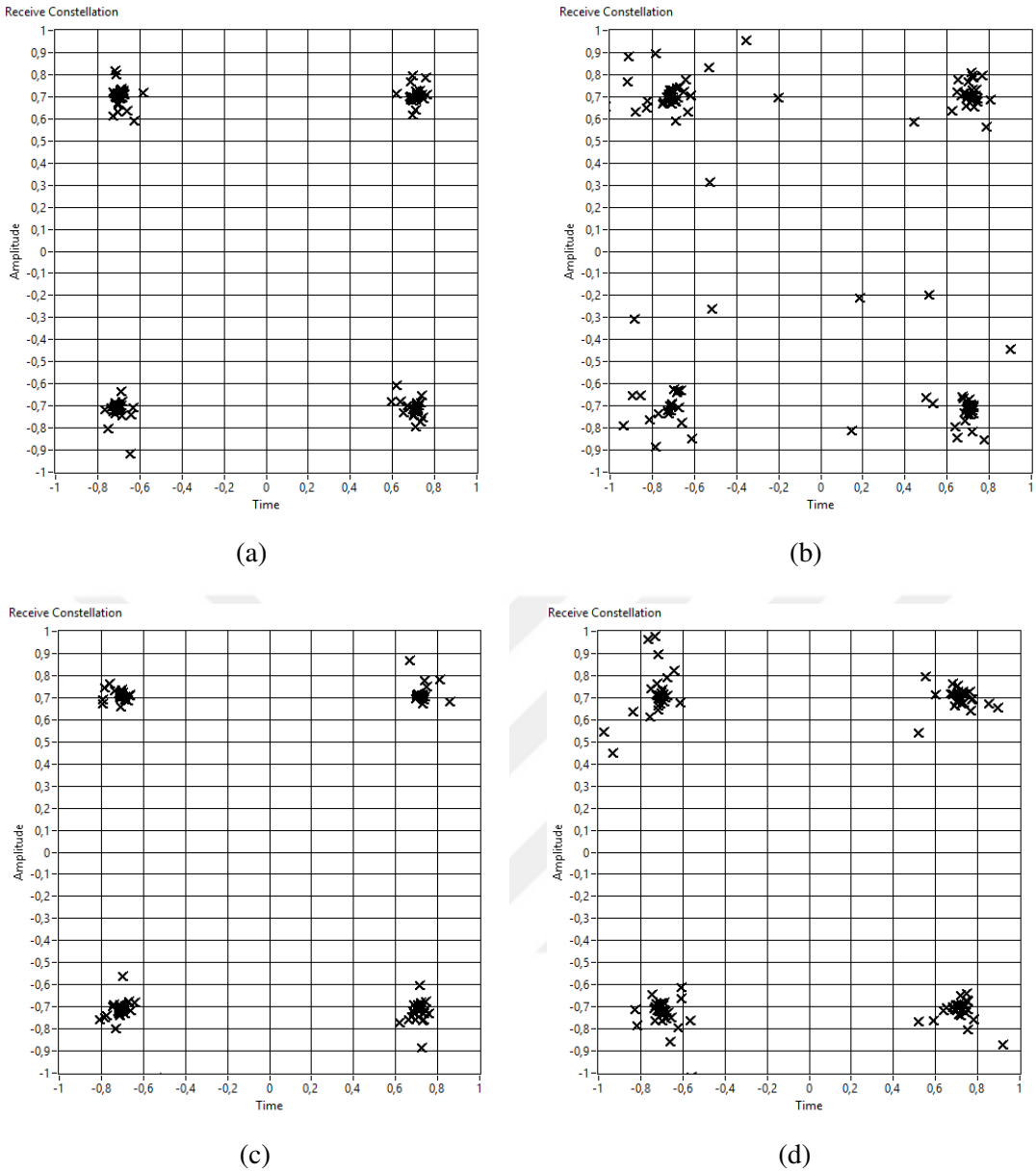

Figure 4.12 : Constellation diagrams with a receive antenna. (a) CP-OFDM. (b) CP-OFDM ($\Psi = 0$ kHz). (c) UF-OFDM. (d) UF-OFDM ($\Psi = 0$ kHz).

In the second scenario, ACI transmitters are included in the tests to generate interference on both sides of the test frequency band. In this scenario, there is no guard band ($\Psi = 0$) between the transmitters. The same waveform is used in each transmitter for a fair comparison. It has been determined that the performance of the CP-OFDM is significantly deteriorated in the presence of ACI and provides an average of ten times worse BER performance. Approximately 8dB interference in the presence of ACI occurs. Under the same conditions, with UF-OFDM, approximately 3 dB ACI is encountered and BER performance worsens on the average by 2 times. UF-OFDM offers much better BER performance than CP-OFDM when no guard band is used.The

constellation diagrams for CP-OFDM and UF-OFDM for the first and second scenarios are shown in Figure 4.12.

In other scenarios, the effect of OoB emissions on the performance of the waveforms is investigated by creating guard bands of 1.5, 3 and 6 kHz, respectively. The increase in CP-OFDM and UF-OFDM performance occurs with the guard band use. UF-OFDM has better performance than CP-OFDM up to 6 kHz guard band usage. The use of 6 kHz guard band in CP-OFDM and zero guard band utilization in UF-OFDM are about the same performance. For this reason, the result of not using guard band in UF-OFDM is that a spectral efficiency of 6 kHz according to CP-OFDM is achieved for the same performance. It has also been understood that the use of UF-OFDM during testing has been performing better in resolving the CFO effect.

4.7 Conclusion

Test results show that CP-OFDM is more successful than UF-OFDM in perfect synchronization and the absence of ACI. However, UF-OFDM has yielded more successful results in the case of imperfect synchronization as in real-time systems. Although, ACI does not have much effective on the UF-OFDM and CP-OFDM especially degrades the edge symbols. In this conclusion, it is observed that UF-OFDM is more robust than CP-OFDM in real-time applications in dense deployment.As future work MIMO extension of the designed test-bed is planned.4

5. SPATIAL MODULATION

5.1 Introduction

In addition to meet the demands of high level users, it is aimed to provide more effective and reliable communication with 5G and mobile communication systems beyond. A lot of studies are being done to the literature in order to contribute to the next generation communication systems. Large data sets are formed with the diversification of the areas of the communication technologies, large data sets resulting from fast developing technologies show an exponential increase and transformed into a lot of data which is very difficult to interpret with human power. From this point of view, in 5G and mobile communication systems beyond, it is aimed to meet big user demands and improve their experience with machine learning techniques with machine learning techniques of data sets.

With the application of highly promising spatial modulation (SM) technique with massive multiple-input multiple-output (MIMO) systems for new generation communication systems, spectral and energy efficiencies are increased to a much higher level [66]. To improve the performance of SM systems, transmitting antenna selection (TAS) was first investigated in [67]. Two TAS methods have been proposed: capacity (COAS) and euclidean distance based antenna selection (EDAS). The EDAS method shows better error performance than the COAS method and has brought high complexity. When other studies in the literature are examined, it has been shown that communication systems can improve error performance by making transmitting antenna selection [68, 69], high energy efficiency [70] and capacity [71] needs can be met. In [68], the authors presented a system with a low complexity that provided the same error performance as Euclid Distance Based Antenna Selection (EDAS). In [69], a method with low complexity was presented for transmitting antenna selection and it has been shown that with the mentioned method, the error performance is more successful than the classical MIMO systems. To improve energy efficiency, in [70], different transmitter antenna selection approaches based on search techniques have

been demonstrated. In [71], two different transmitter antenna selection algorithms are presented which aimed to reduce the number of antennas selected in the transmitter and to maximize the average speed. In [72], a new transmitting antenna grouping scheme has been proposed for generalized spatial modulation and the improvement of the system performance was shown.

In this study, the selection of transmitter antenna in the massive MIMO SM systems is defined as a multi-class classification problem and it has been shown that the system complexity can be reduced by using the appropriate machine learning method. The proposed method has been tested on software-based radio (SDR) nodes and it is seen that massive MIMO SM systems can meet the criteria expected from next generation technologies when applied with machine learning algorithms.

5.2 General Information

5.2.1 Spatial Modulation

Single-carrier spatial modulation (SM-MIMO) comes to the fore as a highly efficient technique, working with switching aid and as a technique which is capable of accomplishing the MIMO system design using a single RF chain in the transmitter [66]. The significant advantages and disadvantages of SM-MIMO are shown in Table [73]. In SM-MIMO, information bits are divided into two parts: modulation bits and antenna bits. Modulation bits can be modulated by any preferred numerical modulation method. In this study, QAM is used as the numerical modulation method, which is often preferred. Antenna bits carries the index information of the antenna to be used. The antenna bits to be sent are determined according to the number of antennas on the transmitter side. Modulated signal formed according to the modulation bits is transmitted from the antenna selected according to the antenna bits. In this way, a MIMO system is created and the coding gain is obtained. The sign schemes for spatial modulation are shown in the Figure 5.1.

In SM-MIMO system, with the help of the largest possible detection process on the receiving side, index information of the antenna where the signal is sent and modulation signal is obtained [73]. When $\mathbb{S} = \{s\}_1^M$ used as set of modulation symbols, $\mathbb{L} = \{i\}_1^{N_t}$ as set of transmitting antennas, s as modulated signal and i as used antenna;

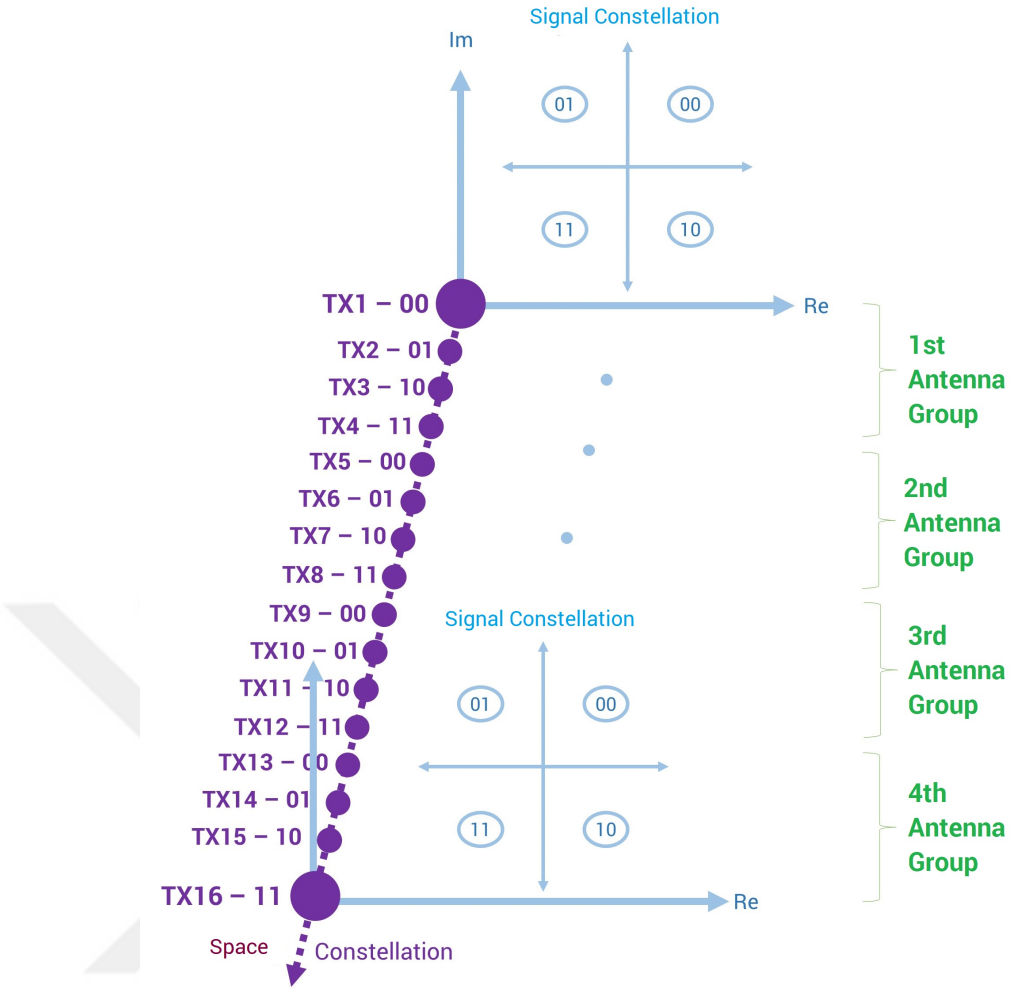

Figure 5.1 : SM constellation diagram for AS.

under the assumption in which channel status information (CSI) is known by the recipient without loss, i and s values obtained by maximum likelihood detection:

$$(\tilde{i},\tilde{s})_{ML} = \arg \min_{i\in\mathbb{L},\, s\in\mathbb{S}} \|\mathbf{y} - \sqrt{\rho}\mathbf{h_i}s\|_2^2 \,. \tag{5.1}$$

Here, $\mathbf{x}$ represents the signal sent from the transmitter, ρ represents the average signal-noise ratio at each receiver antenna and y represents the sign received by the receiver. When, N_t as the number of transmitting antennas; N_r as the receiving antenna number and M as modulation degree; m as the number of bits that can be transmitted instantaneously in the SM-MIMO system:

$$m = \lfloor \log_2(N_t \times M) \rfloor \ \ bpcu. \tag{5.2}$$

Table 5.1 : Advantages and disadvantages of SM.

Advantages	Disadvantages
High data rate	Very fast antenna switching request
Simple receiver design	Time constraint in pulse shaping
Simple transmitter design	the need for all channel information
Reduced power consumption	Redirected beam-forming restriction
Increased spectral efficiency	Minimum two receive antennas

Different approaches are presented in the literature to improve the error performance of the SM-MIMO system. Antenna selection (AS) approach, which is frequently used in general MIMO systems, is also considered as a suitable option for SM-MIMO in terms of error performance. Optimal method to improve error performance is, antenna selection method EDAS which calculates the norm square of the distance between the symbols under the channel state information [68].

$$\varphi_{EDAS} = \arg\max_{\varphi \in \Upsilon} \left\{ \min_{s_1 \neq s_2 \in \mathbb{S}} \|\mathbf{H}_{\varphi}(\mathbf{x}_1 - \mathbf{x}_2)\|_2^2 \right\} \tag{5.3}$$

Although AS provides improvement in error performance, it causes loss in spectral efficiency. In order to perform AS, T in the SM-MIMO system is divided into at least two groups and causes a loss of at least 1 $bpcu$. Despite the increase in the number of groups and thus the loss of $bpcu$, error performance is improved with AS.

5.2.2 K nearest neighborhood (k-NN)

The nearest neighborhood algorithm is a non-parametric, controlled learning method used for classification and regression. Consider in t_0 to be the test sample, k-NN classifier first identifies the nearest K neighbor data sample and calculates the probability that the test data belongs to any class.

$$Pr(V = j | T = t_0) = \frac{1}{K} \sum_{c \in N_0} I(v_c = j) \tag{5.4}$$

Here the cluster which contains the classes of the neighboring data sample which is closest to N_0 test data, represents j class information. k-NN classifier classifies t_0 test observation to the highest probability class.

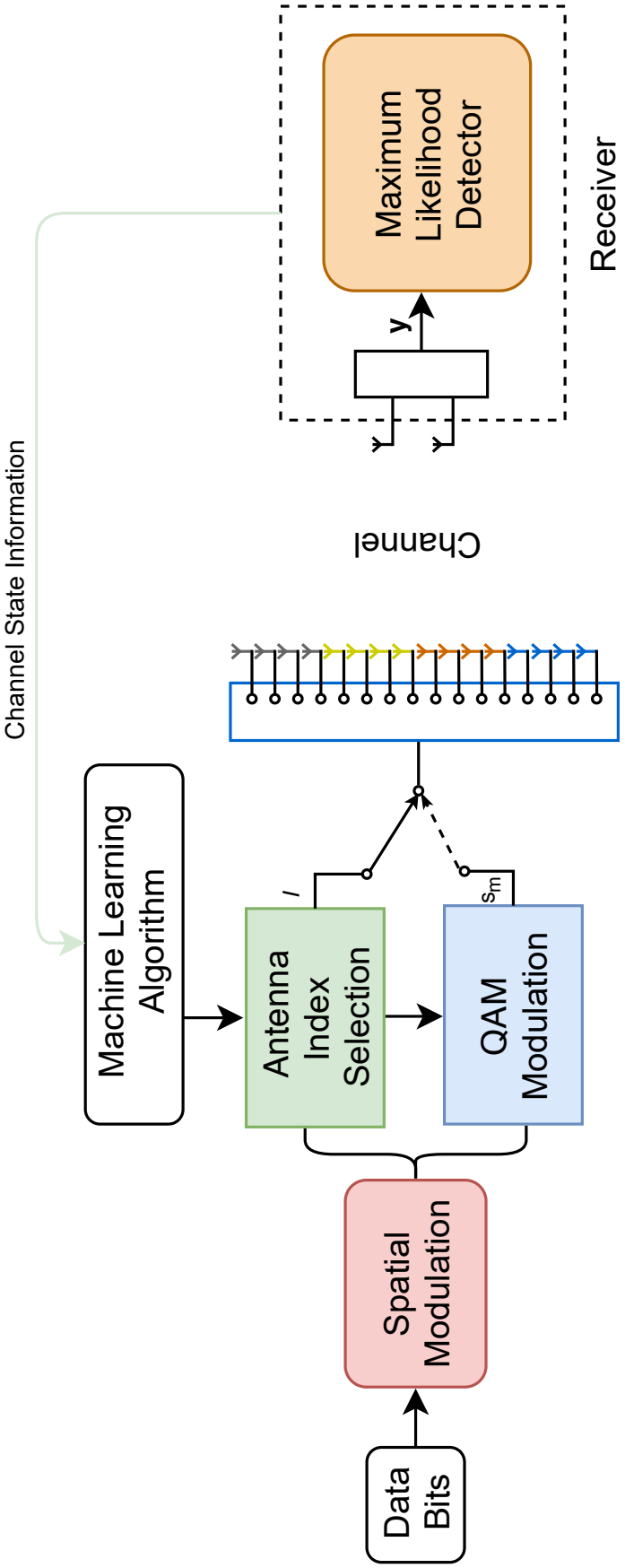

Figure 5.2 : SM antenna selection system with machine learning approach.

5.3 System Design

5.3.1 Generation of the data set

6 different data sets, 3 for each have been created by using simulation and real-time systems to be used in training and testing phases of k-NN algorithm. All data sets are labeled according to the Euclidean distance based antenna selection approach. Data set obtained by simulation method: 1 million training data consists of 1 million test data. Data set generated from a real-time massive MIMO system: 5 million training consist of 5 million test data. 16 transmit antenna units are divided into groups of 2, 4 or 8 thus each group will independently make SM. The transmission is provided via the antenna of the selected antenna group. For each group, channel status information is collected and defined as a property in the data set.

5.3.2 Real-time massive MIMO SM system

In the recommended test system, eight USRP-2943R devices with two RF chains in the transmitter and USRP-2940 devices with two RF chains in the receiver have been used as SDR node. As software, LabVIEW was preferred which is one of the graphical programming languages and which performs highly efficient communication with USRP devices. In order to ensure the synchronization of 16 channel, ls in the transmitter ”NI PXIe-6674T Synchronization Module“ which produces reference clock and “CDA-2990 eight-channel clock distribution module” which shares this clock information to all devices were used as tools. USRP-2940 device on the receiver, performs synchronization process in itself. The management of USRP devices in the receiver and transmitter can usually be controlled via the same computer. Any communication system designed in the base band can be operated in real-time with the desired carrier frequency and bandwidth under hardware restrictions with USRP. System parameters are shown in the table.

The USRP has basically a local oscillator, FPGA in which the digital signal processing is carried out, analog and digital converters (ADC and DAC), and low-pass filters. Due to its modular structure, USRP can be easily evaluated for different purposes. The USRP 2943R used in the tests can be used in a maximum 16-bit sampling interval and 40 MHz bandwidth and operates in the 1.2 GHz to 6 GHz frequency range and can

Table 5.2 : System parameters.

Carrier Frequency	2.2 GHz
Modulation	4-QAM
Tx Gain	5, 10, 15 dB
Rx Gain	0 dB
N_t	16
N_r	2
Subset	2, 4, 8
Distance	3 metre
IQ Rate	2 MS

produce up to 20 dBm of signal. The operating frequencies of the USRP 2940 range from 50 MHz to 2.2 GHz. In this study, the operating frequency for two different devices is determined as 2.2 GHz.

The common problem of real-time tests is the difficulty of synchronization between the receiver and the transmitter. The problem of carrier frequency drift (CFO) and sample time drift (STO) because of various reasons between the receiver and the transmitter can be eliminated with the help of pilot sequences which are placed at certain frequencies to the signal [74]. In this study, the system designed as detailed in [73] was used.

Although a single RF chain is used in SM system in general terms, different RF chains are used instead of switching in the recommended system for testing purposes. Although the number of antennas used in transmission is 16, because of the antenna selection, the number of bits transmitted from the antenna is set to 2 instead of 4 and for this reason, 4 different antenna options have been created which are transmitted by antenna information and expressing 2 bits. As a modulation method, QAM was preferred in the system formed as a single carrier. Antenna selection was realized by machine learning method and similar performance has been achieved with EDAS, which is the method that optimizes error performance. The real-time system used in the tests is shown in the Figure 5.3.

5.4 Results

In this study, the performance of antenna selection which are highly effective in the performance of massive MIMO systems by using k-NN machine learning algorithm in

Figure 5.3 : Proposed test-bed.

real-time and simulation testing environments is examined. Simulation results showing the effect of antenna selection on error performance are shown in the Figure 5.4.

Table 5.3 : k-NN AS accuracy results.

Data Set	**4 Group**	**4 Group**	**2 Group**
Simulation Results	0.933258	0.98699	0.999508
Real-time Results	0.999931	0.993792	0.999453

According to the simulation and real-time test results, the performance table which was created with the results obtained according to EDAS which is an important metric in error performance and with the comparison of the results obtained with the machine learning method k-NN is given in the Table 5.3.

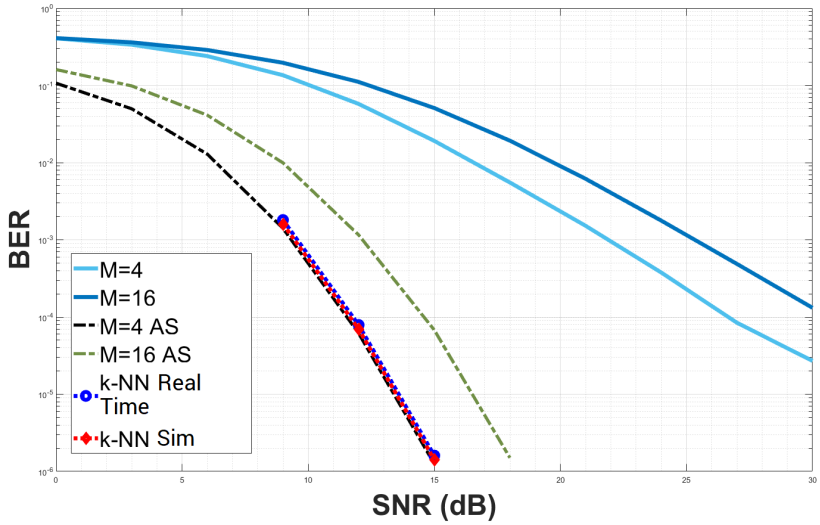

Figure 5.4 : Error performance of antenna selection.

According to the simulation results, it is seen that the performance of k-NN algorithm decreases as the number of groups increases. According to the real-time test results, it is seen that performance has no linear relationship with the number of groups and k-NN algorithm shows a result which is very close to perfection in real-time. The most important reason for the difference between the simulation and real-time results when the number of groups increases is the prediction that the channel structure in the simulation environment is independent and distributed in the same way. However, in the real-time test environment, it is understood that the variance of the channel varies less than an independent and uniformly distributed channel structure and therefore the performance rates obtained are very close to perfection.

5.5 Conclusion

Massive MIMO SM systems are among the techniques which have the potential to meet the targeted energy and spectral efficiency criteria in 5G and beyond communications systems. In this statement, machine learning-based approach has been suggested while improving the performance of massive MIMO SM systems with the selection of transmitting antenna. While the method has almost the same performance as the optimum method, it has been shown to be more applicable in real-time systems than classical methods with its lower complexity feature.

6. GENERALIZED SPATIAL MODULATION

6.1 Introduction

The variability and the diversity of user expectations increase functionality requirements of wireless communication systems. In 5G mobile broadband systems, it is aimed to improve the functionality of the systems as well as the capacity and the coverage. Massive multiple input multiple output (Ma-MIMO) technology is considered as one of the key techniques to address reliability, spectral and energy efficiency objectives of such systems [75].

Ma-MIMO systems with antenna selection (AS) methods provide a better performance by using the different channels between transmitter and receiver [76]. The authors of [77] propose two transmit AS methods: capacity-optimized antenna selection (COAS) and Euclidean distance-optimized antenna selection (EDAS). The EDAS method attains a higher diversity gain and a better bit error rate (BER) performance with a higher complexity. However, application of these methods in real-time systems is restricted by the complexity and flexibility requirements of next-generation communication systems. At this point, advances in machine learning techniques promise to leverage advantages of Ma-MIMO technologies. In [78, 79], AS problem is characterized as a multi-class classification problem, which enables to utilize machine learning based schemes. In [78], optimization-driven and data-driven AS methods are evaluated in terms of complexity and performance. In [79], machine learning methods are implemented to select the optimal antenna that maximizes the secrecy performance.

Generalized spatial modulation (GSM) is a practical candidate for Ma-MIMO systems due to its higher spectral efficiency and the convenience for flexible design [80]. In [80], a novel transmit antenna grouping scheme is proposed, improving the performance relative to the conventional GSM. The authors of [81] show that GSM can achieve a better performance than spatial multiplexing when the optimum antenna combination is selected.

In this chapter, we propose to provide a dynamic and flexible structure for Ma-MIMO systems. We propose to utilize machine learning methods for GSM to improve the flexibility of Ma-MIMO systems. The contributions of the chapter can be summarized as follows:

- We implement GSM using the applicability of machine learning methods is shown in the real-time environment.
- We utilize two machine learning based approaches, the decision tree (DT) and the multi-layer perceptron (MLP), for antenna subset selection in GSM under imperfect channel state information (CSI).
- We analyze the performance of proposed schemes numerically and experimentally, through the designed real-time software defined radio (SDR) based test-bed with 16×4 MIMO channel.

Both machine learning based approaches provide better performances than the conventional AS method in terms of BER under non-ideal but realistic transmission scenarios. Simulations, as well as real-time test results, have shown that EDAS method is very successful when the channel is perfectly known. Otherwise, our proposed schemes based on machine learning provide a superior error performance, which is demonstrated by simulations and real-time tests.

6.2 System Model

GSM can be considered as an adjustable extension of the spatial modulation where an antenna index refers a different spatial symbol to convey more information [80]. The proposed Ma-MIMO GSM system has N_t transmit antennas and N_r receive antennas. The number of active transmit antennas is denoted by N_u, and I_A is the spatial symbol. The maximum number of spatial bits can be transmitted is $\lfloor \log_2 C \rfloor$, where $C = \binom{N_t}{N_u}$, is the number of combinations and $\lfloor \cdot \rfloor$ denotes the floor operator. GSM eliminates the necessity of N_t being power of 2 and provides a more flexible usage of the system. The block diagram of the GSM system is shown in the Figure 6.1 and the designed test-bed is shown in 6.2. We assume that the same symbol is transmitted through all active antennas as in [82] and the maximum number of bits that can be transmitted is

$\log_2 M + \lfloor \log_2 C \rfloor$ bits per channel use $(bpcu)$, where M is the modulation order. The communication channel is denoted by, $\mathbf{H} \in \mathbb{C}^{N_r \times N_t}$ where $\mathbf{H^T} = [\mathbf{h}_1, \cdots, \mathbf{h}_r, \cdots, \mathbf{h}_{N_r}]$ and $\mathbf{h}_r = [h_{r,1}, h_{r,2}, \cdots, h_{r,N_t}]$. The received signal vector is as $\mathbf{y} = \mathbf{H}\mathbf{x} + \mathbf{w}$, where $\mathbf{w} \in \mathbb{C}^{N_r \times 1}$ is the additive white Gaussian noise component [75]. $\mathbf{x} = s_\zeta \mathbf{I}^C$ represents the GSM symbol, where s is the ζ^{th} modulation symbol, $\mathbb{S}$ is symbol cluster, $I_t^C \in \{0,1\}$ and $\mathbf{I^C} = [I_1^C, I_2^C, \cdots, I_{N_t}^C]^\top \in \mathbb{I}$ is transmit antenna combination vector, $\mathbb{I}$ denotes combination cluster. To represent the evolution from theoretical to practical systems; both perfect and imperfect channel estimates, and correlated and independent and identically distributed *(i.i.d)* channel models are considered. The imperfect channel is [83]:

$$\widehat{\mathbf{H}}_\nu = \sqrt{1-\beta}\mathbf{H}_\nu + \sqrt{\beta}\mathbf{E}_\nu, \tag{6.1}$$

where ν is the time index, $\beta \in [0,1]$ is the channel estimation error coefficient, $\mathbf{H}_\nu$ is the channel matrix and $\mathbf{E}_\nu$ denotes the estimation error matrix at time ν. The time-correlated channel is modelled as [84]:

$$\mathbf{H}_\nu = \sqrt{\alpha}\mathbf{H}_{\nu-\iota} + \sqrt{1-\alpha}\mathbf{Z}_\nu, \tag{6.2}$$

where ι is the time offset, $\alpha \in [0,1]$ is the time correlation coefficient, and $\mathbf{Z}_\nu$ denotes the time-correlation error matrix. Both of $\mathbf{Z}_\nu$ and $\mathbf{E}_\nu$ are complex normal distributed with zero mean and unit variance. Recalling (6.1) and (6.2), the imperfect time-correlated channel estimate is modelled as follows:

$$\widehat{\mathbf{H}}_\nu = \sqrt{(1-\beta)\alpha}\mathbf{H}_{\nu-\iota} + \sqrt{(1-\alpha)(1-\beta)}\mathbf{Z}_\nu + \sqrt{\beta}\mathbf{E}_\nu, \tag{6.3}$$

The maximum likelihood detector is preferred at the receiver to identify the modulation and the spatial symbols. The CSI must be accurately known for the best performance of the maximum likelihood detector. In GSM system designs, frequently it is assumed that CSI is known perfectly at the receiver and the performance is improved under this assumption. The maximum likelihood detector is:

$$(\hat{\mathbf{I}}^C, \hat{s}_\zeta) = \arg\min_{\mathbf{I}^C,\, s_\zeta} \sum_{i=1}^{N_r} \left| y_i - s_\zeta \mathbf{h}_i \mathbf{I^C} \right|^2, \tag{6.4}$$

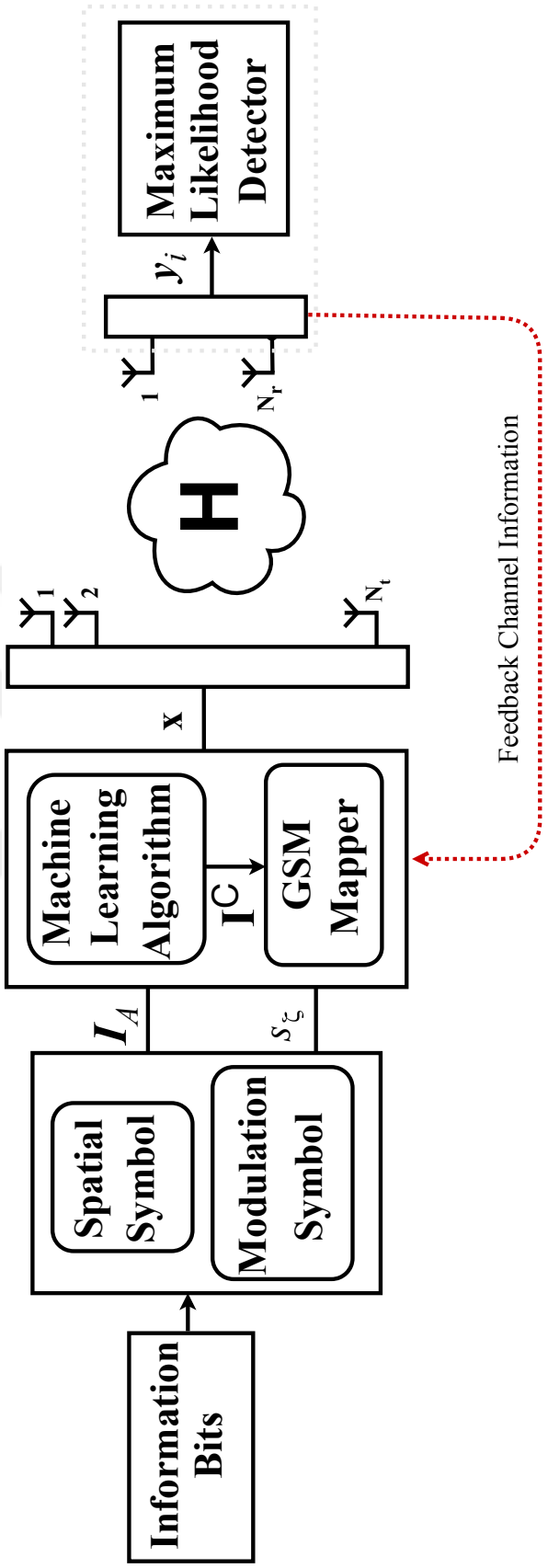

Figure 6.1 : The proposed machine learning based AS scheme for Ma-MIMO GSM.

where y_i is the received symbol at the i^{th} receive antenna. The AS approach, which is frequently used in general MIMO systems, is seen as a suitable option for GSM in terms of error performance. The conventional method for improving error performance is EDAS, which calculates the norm square of the distance between the symbols. A subset κ determined by EDAS is:

$$\kappa_{EDAS} = \arg\max_{\mathbf{I}^{\mathbf{C}} \in \mathbb{I}} \left\{ \min_{s_1 \neq s_2 \in \mathbb{S}} \left| (s_1 - s_2) \sum_{i=1}^{N_r} \mathbf{h}_i \mathbf{I}^{\mathbf{C}} \right|^2 \right\} \tag{6.5}$$

Although AS provides an improvement in the error performance, it causes a loss in spectral efficiency. The total number of subsets is $L = \lfloor \frac{C}{2^\rho} \rfloor$, where ρ is the number of bits in a spatial symbol. In order to be able to perform AS, the C in the GSM system is divided into at least two subsets, causing a loss of at least 1 $bpcu$. Despite the increase in the number of groups and thus the loss of spectral efficiency, the error performance is improved.

6.3 Proposed Schemes

6.3.1 Data set acquisition

According to the model in Figure 6.1, three different cases are considered and three data sets are built. Two simulation based data sets are created depending on equations (6.1) and (6.3) to resemble the conditions of real-time systems. The third data set is generated on real-time test-bed. $\mathbf{X} \in \mathbb{R}^{N \times Q}$ and $\mathbf{X} = [\mathbf{x}_1\ \mathbf{x}_2\ ...\ \mathbf{x}_{N-1}\ \mathbf{x}_N]^T$ represents a data set, where N is the number of samples and Q is the total number of features. Data sets are generated with three features based on channel matrices and error vector magnitudes for each subset. An instance is designed as $\mathbf{x}_n = [f_{n,1}\ f_{n,2}\ ...\ f_{n,Q}]^T$, for $n = 1, 2, \cdots, N$. Three features are extracted for all subsets as follows:

$$f_{n,q} = \begin{cases} \sum_{t=1}^{N_t} \sum_{r=1}^{N_u} |h_{r,t}|^2, & \text{if } q = 1, \cdots, L \\ \frac{\frac{1}{N} \sum_{n=0}^{N-1} \varepsilon}{P_S} \times 100, & \text{if } q = (L+1), \cdots, 2L \\ f_{n,q-2L} - f_{n-\delta,q-2L}, & \text{if } q = (2L+1), \cdots, Q \end{cases} \tag{6.6}$$

where L is the total subset number, P_S is the average symbol power, ε is the error power and δ is the feedback delay. Note that α and β are not necessary for the DT and the MLP based AS schemes. Each class represents an antenna subset to transmit a spatial symbol. The duration of data collection via the real-time test-bed is set to 7 seconds. All data sets are split as training and test data sets and they contain 2 and 2.5 millions samples, respectively. The conventional method in terms of error performance, EDAS, is used to label each data sample based on (6.5).

6.3.2 Learning algorithms

The success of learning algorithms especially, deep neural networks, is explicit in a variety of disciplines [80], leading to their frequent utilization in a wide range of applications in the recent years. The received samples from a communication system can include outlier data samples, due to the inherent imperfections of the communication systems, such as erroneous channel estimates. The use of learning techniques can aid combat these imperfections. The selection of robust algorithms and building appropriate models against outliers are critical issues to improve the target the performance criterion. The complexity levels of the selected learning algorithms must also be taken into account. Here, we focus on DT and MLP. The DT comes into prominence with its lower complexity, making it more practically applicable. However, the simpler structure of the DT restrains its performance. The MLP is capable of capturing the nonlinear relationship in a dataset. As a result of this, it has the ability to handle more complex data with multiple layers between the input and the output, at a cost of increased complexity.

6.3.2.1 Decision tree

By creating decision rules based on statistical information of the training data set, DT targets to correctly estimate the class of the new sample [85]. The DT is composed of three basic units as root, branch and leaf nodes. The prediction complexity of DT can be defined as $O(Q)$ [86, 87]. The features maximize the information gain on each node is determined by using (6.7) and (6.8). The node is divided into child nodes depending on the selected features as:

$$\Upsilon_m = -\sum_{\kappa=1}^{L} p_m^{\kappa} \log_2 p_m^{\kappa} \,, \tag{6.7}$$

where $p_m^{\kappa} = N_m^{\kappa}/N_m$ represents the probability of the κ^{th} class on the m^{th} node, N_m is the number of data samples, N_m^{κ} shows the probability of samples belonging to κ^{th} class on m^{th} node, Υ_m is the entropy of the m^{th} node. On the each node for determining the feature which provides maximum information gain,

$$\Psi(m, \mathbf{f}_q) = \Upsilon_m - \sum_{d=1}^{D} p_d \Upsilon_d \tag{6.8}$$

is used, where $\mathbf{f}_q$ is the q^{th} feature, Ψ is the information gain related to $\mathbf{f}_q$ on the m^{th} node and d shows the number of child nodes on the m^{th} node, p_d is the probability of the corresponding child node.

6.3.2.2 Multi-layer perceptron

MLP is an artificial neural network structure and has the ability to learn non-linear functions via a given set of features. MLP is a considerably successful method, even though it has a higher computational complexity compared to DT. The prediction complexity of MLP is approximately defined as $O(Q\text{ł}_1 + \text{ł}_1\text{ł}_2 + \cdots + \text{ł}_\mu\text{ł}_{\mu+1})$, where ł_μ is the number of neurons at μ^{th} layer [86, 87]. It consists of three main layers; input layer, hidden layers and output layer. The MLP is trained with adaptive moment estimation (ADAM) optimizer by using backpropagation algorithms through neurons at these layers. On the training of the model, cross entropy $J(\Theta)$ is used as a cost function as given in [86]:

$$J(\Theta) = \frac{-1}{N} \sum_{n=1}^{N} \sum_{\kappa=1}^{L} \gamma_n^{\kappa} \log \rho_n^{\kappa}, \tag{6.9}$$

where N is the number of instances and ρ_n^{κ} is the estimated probability that the instance $\mathbf{x}_n$ belongs to class κ. γ_n^{κ} is equal to 1 if the target class for the n^{th} instance is κ. Otherwise, it is equal to 0. The hyperparameters of the training phase are determined empirically.

6.4 Test-bed Design

The test-bed is designed as shown in Figure 6.2. We use USRP devices as SDR nodes with two RF chains. We prefer to use distinct RF chains instead of switching for the

purpose of testing. As a software, LabVIEW is used. 4-QAM modulation is selected. For data transmission we set $N_t = 12$ and $N_r = 2$, two modules are utilized to provide hardware synchronization of the 12 transmit channels: PXIe-6674T and CDA-2990. A reference clock is generated firstly with the PXIe-6674T module and the clock information is shared with all devices by the CDA-2990. The first USRP-2940 is used as the Ma-MIMO GSM receiver. The second USRP-2940 is used to feed the estimated CSI to the transmitter. At the transmitter side, two USRPs are allocated to receive the feedback channel information. The maximal ratio combining is preferred to restore the CSI feedback. We analyze only the existence of channel estimation errors. For this reason, feedback channel signals are designed to operate at a high the signal to noise ratio (SNR), approximately 30 dB. In this study, operating frequency for transmitter channels and the operating frequency for feedback channels are determined as 2.1 GHz, 2 GHz, respectively. The average SNR values in real-time tests are calculated with the equivalent signal power to compare with the simulation results. The transmitter power levels used in the real-time test system are varied between -10 dBm and 10 dBm. Symbol data rate is 2 Msample/sec. When the antenna selection is used, spectral efficiency and the data rate of the system are 5 *bpcu* and 10 Mbps, respectively. The carrier frequency offset and sample timing offset problems between the receiver and the transmitter are eliminated by the pilot sequences are used.

6.5 Results

In Ma-MIMO GSM system, the performances of the proposed machine learning based AS methodologies and EDAS are analyzed numerically and in the real-time environment. EDAS has the highest diversity gain. MLP, which provides a better diversity gain than DT, shows a similar performance to EDAS. EDAS has the best diversity gain. MLP, which provides a better diversity gain than DT, is also slightly close to EDAS. The values of α and β are chosen in accordance with the measurements on the real-time test-bed, where $\alpha \approx 0.66$ and $\beta \approx 0.1$. The channel of the test environment is estimated as a Ricean channel with $K \approx 5$. The error performances of the simulation environment in the Rayleigh fading channel are obtained with varying α and β parameters are shown in Figures 6.3 and 6.4. 8 different antenna subsets are created by setting ρ and N_u are to 3 and 2. The training datasets are used to fit models

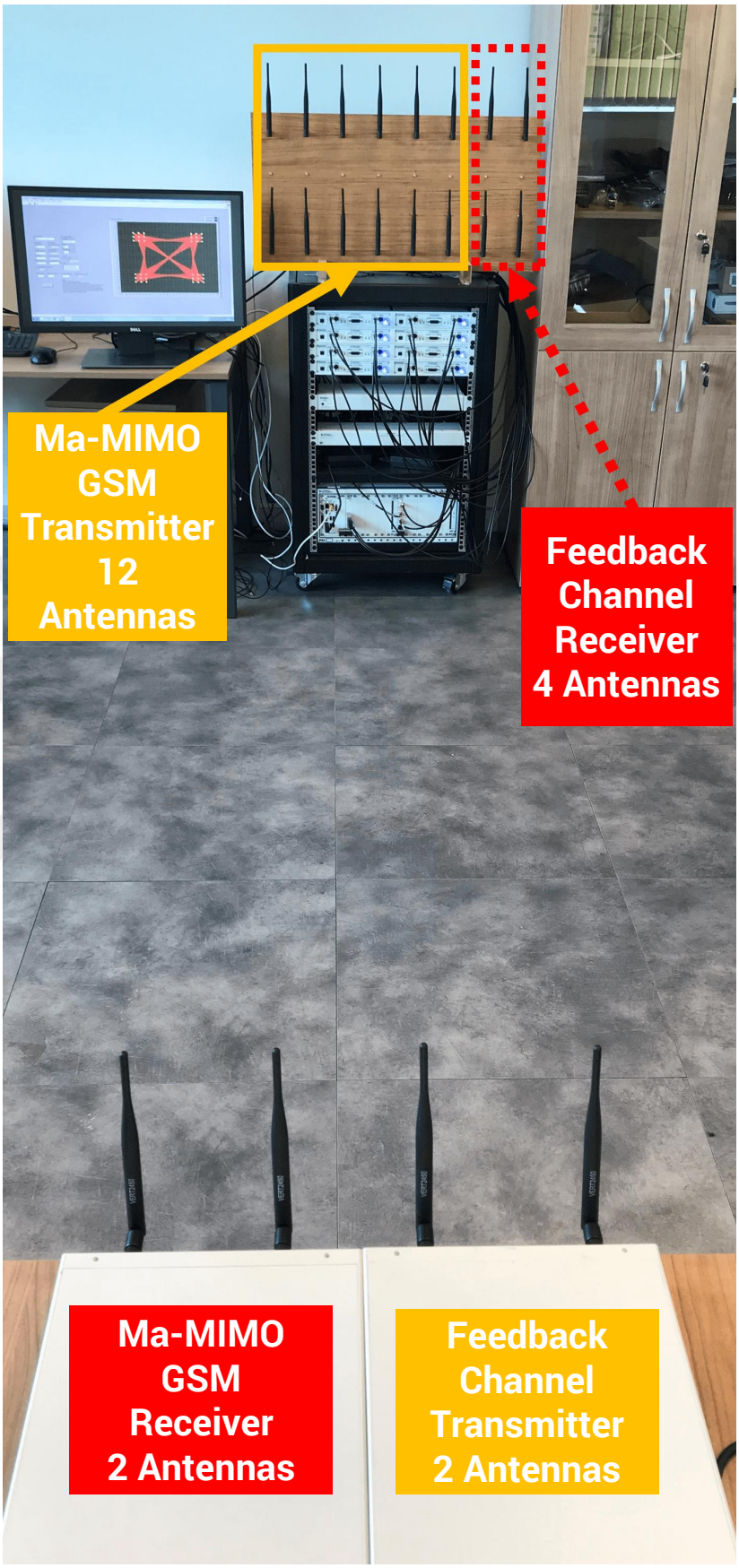

Figure 6.2 : The real-time 16×4 test-bed.

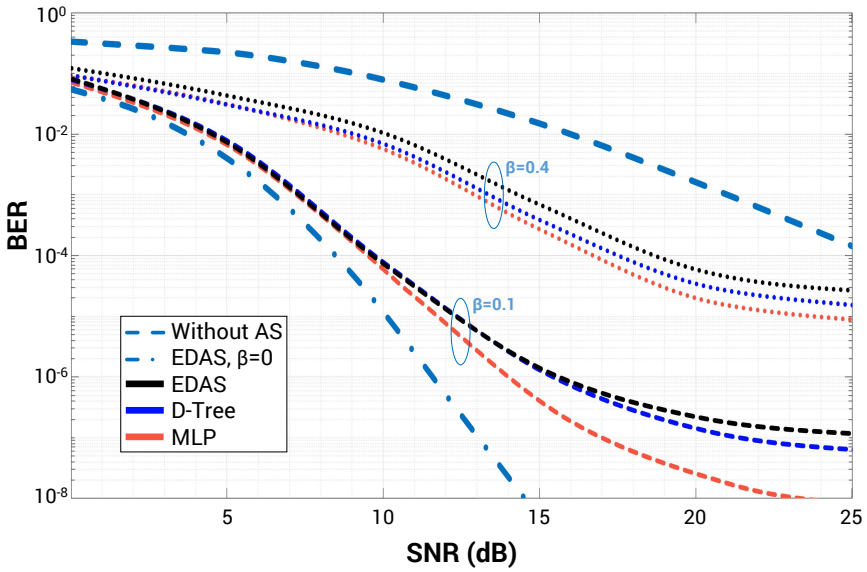

Figure 6.3 : Simulation results for the (*i.i.d.*) channel under the channel estimation errors.

and parameters are determined empirically for the two learning algorithms during the training. The models in this study are built using Python. The depth of the DT model, the number of the MLP model's hidden layers and the number of neurons at one layer are set to 17, 2, 15, respectively. Then, the constructed models are stored and tested.

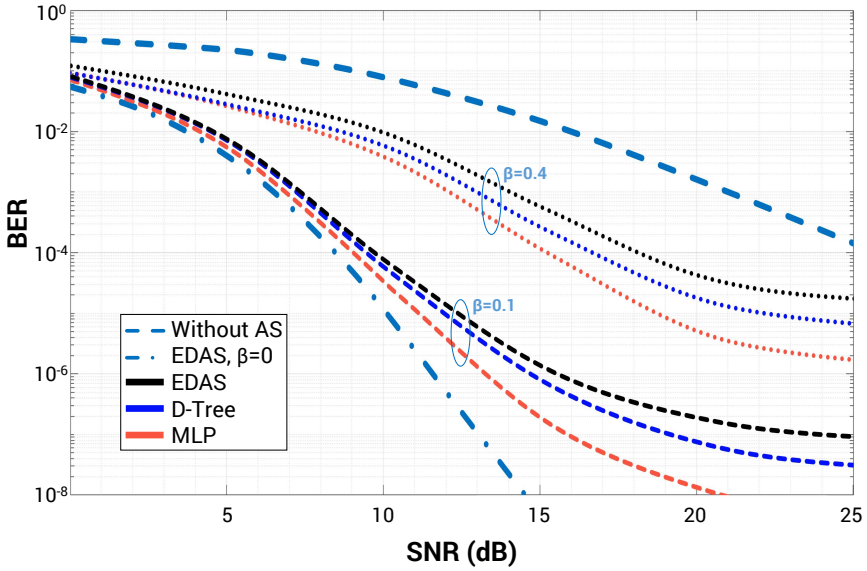

Figure 6.4 : Simulation results for the time-correlated channel ($\alpha \approx 0.66$) and the channel estimation errors.

Figures 6.3, 6.4 and 6.5 show the comparison of the machine learning based AS and EDAS schemes. All methods perform better than the case without AS in terms of BER. The performance of EDAS is reduced significantly when β increases. The

MLP based AS scheme achieves a higher performance for all cases because of the more sensitive construction to the features. The DT based scheme outperforms EDAS with an acceptable error performance but its simpler structure leads to missing some hard-to-discern patterns in the dataset when compared to MLP. Also, MLP appears to be more advantageous against the impact of the time-correlation on the channel. The results of the real-time tests are shown in Figure 6.5. EDAS shows a weak performance due to the delayed imperfect CSI. The performance of EDAS increases and converges to the perfect CSI boundaries as the estimation error is reduced for the high SNR values. Although EDAS and DT performances are similar for high SNR values. DT shows a higher performance compared with EDAS when SNR decreases in real-time tests.

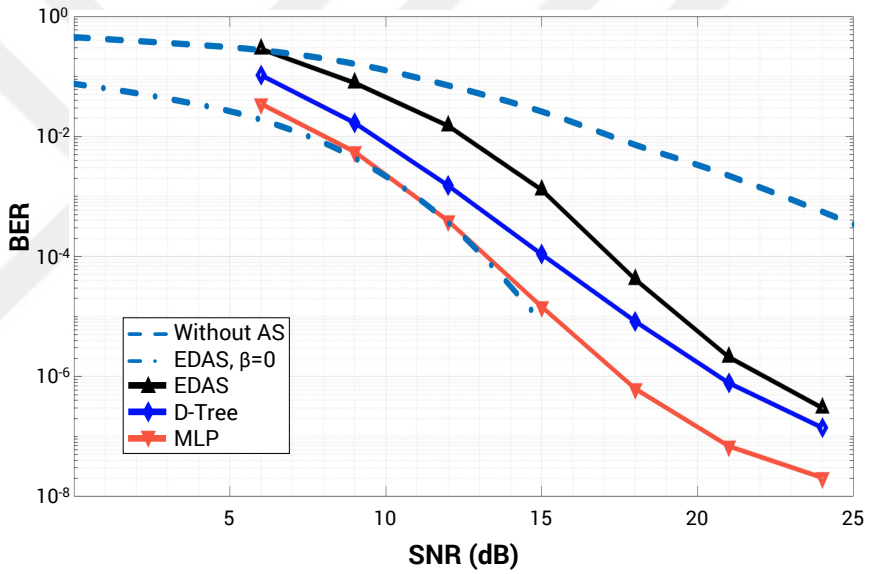

Figure 6.5 : Real-time system results.

Additionally, the computation duration of each AS scheme is measured for an instance under the same conditions to investigate the impacts of the approaches in terms of time-complexity. The lengths of test-time for the MLP, EDAS, the DT based schemes are 16 nanoseconds (ns), 10 ns, 8 ns, respectively. The MLP achieves lower error rates than DT but it is a more complex method, which slows down the test system in real-time. As seen from Figure 6.5, machine learning approaches provide a robust performance in the presence of imperfect CSI and/or delayed CSI when compared to EDAS and decrease BER. Figures 6.3, 6.4 and 6.5 show that the proposed machine

learning based methods have a better performance when compared to the EDAS, in scenarios where channel estimation errors and time-correlated channels are present.

6.6 Conclusions

The spectral efficiency and energy efficiency of the wireless systems can be improved by using GSM technology. In this paper, Ma-MIMO GSM is implemented in a real-time test-bed for the first time in the literature. The performance of the EDAS scheme is evaluated. In order to improve the performance in realistic deployment scenarios, mainly targeting correlated channels and the imperfect channel estimates, a machine learning based framework is proposed for the transmitter. Through simulation and test results, the error performances of the investigated schemes are compared, demonstrating the efficacy of the machine learning based approaches in the presence of real-life impairments.

7. CONCLUSIONS AND RECOMMENDATIONS

In this thesis, CP-OFDM and UF-OFDM waveforms, SM and GSM modulation schemes and NOMA multiple access technique are evaluated from different perspectives in order to meet the user expectations for B5G. The focus of this thesis is to contribute to the most needed energy efficiency and spectral efficiency research for B5G. The common point of all the methods chosen is that they are able to provide energy and spectral efficiency in a good way. Methods examined during the thesis are being investigated on different communication system designs such as SISO, SIMO and MIMO.

NOMA, which is a multiple access technique, allows different users to use the same frequency band in the same period, unlike the orthogonal multiple access (OMA) methods, which are frequently used nowadays. NOMA, which provides spectral efficiency, has been examined in the scope of this thesis both in the simulation environment and in real-time test environment with relayed and without relayed system designs. The advantages and disadvantages of these systems are shown by different parameters. According to the literature research of the author, the relayed NOMA system was realized for the first time in the real-time test environment in this thesis.

UF-OFDM, which is developed as a solution to CP-OFDM's synchronization and side-band problems and based on the principle of filtering of sub-carriers in groups, is first examined in terms of spectral efficiency within the scope of the thesis. SISO and SIMO systems were evaluated from the perspective of CP-OFDM and UF-OFDM spectral efficiency in both simulation and real-time test environment. As a result of the studies, UF-OFDM has similar error performance with CP-OFDM; however, it was found to be a more effective technique in terms of spectral efficiency at the same bit error rate level. In terms of ease of use and performance of spectral efficiency, UF-OFDM has been shown to be preferred in future communication systems.

Spatial modulation schemes using single-carrier modulation, interest in the spectral efficiency and energy efficiency in terms of future communication systems. In the

scope of the thesis, the first time in the literature, SM has been implemented in the massive-MIMO real-time test system. EDAS, an optimum antenna selection method that improves error performance, has been integrated into the SM system and its performance is evaluated in both simulation and real-time test environment. Within the scope of the thesis, k-NN, which is one of the machine learning methods that can be used as an alternative to EDAS, is proposed as the AS method for SM. In the studies conducted, it was determined that the proposed new method showed a good performance.

Unlike spatial modulation, the GSM, which uses multiple RF chains, has been examined within the scope of this study due to its spectral efficiency, flexibility and energy efficiency. GSM has been implemented for the first time in the literature in the real-time test environment. In the test system, GSM performance under imperfect-CSI was evaluated in both simulation environment and real-time test environment. The effect of EDAS method on error performance in GSM system was also investigated. Imperfect-CSI does not provide the desired performance under the EDAS, machine learning methods D-Tree and MLP is recommended. The proposed methods are also applied in real-time test system and they are more successful than EDAS.

All the techniques used in this thesis were chosen because they are effective in terms of energy efficiency and spectral efficiency for B5G. In future studies, different wave-forms, different modulation schemes, different multiple access methods can be examined. In the thesis study, all methods were investigated not only in the simulation environment but also in the real-time test environment. By increasing the number of scenarios created, the advantages and disadvantages of the determined methods from different perspectives can be determined in more detail in future studies.

REFERENCES

[1] **Nakamura, T.**, **Benjebbour, A.**, **Kishiyama, Y.**, **Suyama, S. and Imai, T.** (2015). 5G radio access: Requirements, concept and experimental trials, *IEICE Transactions on Communications*, *98*(8), 1397–1406.

[2] **Welch, T.B. and Shearman, S.** (2012). Teaching software defined radio using the USRP and LabVIEW, *2012 IEEE International Conference on Acoustics, Speech and Signal Processing (ICASSP)*, IEEE, pp.2789–2792.

[3] **Ding, Z.**, **Lei, X.**, **Karagiannidis, G.K.**, **Schober, R.**, **Yuan, J. and Bhargava, V.K.** (2017). A survey on non-orthogonal multiple access for 5G networks: Research challenges and future trends, *IEEE Journal on Selected Areas in Communications*, *35*(10), 2181–2195.

[4] **Islam, S.R.**, **Avazov, N.**, **Dobre, O.A. and Kwak, K.S.** (2016). Power-domain non-orthogonal multiple access (NOMA) in 5G systems: Potentials and challenges, *IEEE Communications Surveys & Tutorials*, *19*(2), 721–742.

[5] **Benjebbour, A.**, **Saito, K.**, **Li, A.**, **Kishiyama, Y. and Nakamura, T.** (2016). Non-orthogonal multiple access (NOMA): Concept and design, *Signal processing for 5G: Algorithms and implementations*, 143–168.

[6] **Kara, F. and Kaya, H.** (2018). BER performances of downlink and uplink NOMA in the presence of SIC errors over fading channels, *IET Communications*, *12*(15), 1834–1844.

[7] **Aldababsa, M.**, **Toka, M.**, **Gökçeli, S.**, **Kurt, G.K. and Kucur, O.** (2018). A tutorial on nonorthogonal multiple access for 5G and beyond, *Wireless Communications and Mobile Computing*, *2018*.

[8] **Wei, X.**, **Liu, H.**, **Geng, Z.**, **Zheng, K.**, **Xu, R.**, **Liu, Y. and Chen, P.** (2016). Software defined radio implementation of a non-orthogonal multiple access system towards 5G, *IEEE Access*, *4*, 9604–9613.

[9] **Xiong, X.**, **Xiang, W.**, **Zheng, K.**, **Shen, H. and Wei, X.** (2015). An open source SDR-based NOMA system for 5G networks, *IEEE Wireless Communications*, *22*(6), 24–32.

[10] **Pan, H.**, **Lu, L. and Liew, S.C.** (2017). Practical power-balanced non-orthogonal multiple access, *IEEE Journal on Selected Areas in Communications*, *35*(10), 2312–2327.

[11] **Wei, X.**, **Geng, Z.**, **Liu, H.**, **Zheng, K. and Xu, R.** (2017). A portable sdr non-orthogonal multiple access testbed for 5g networks, *2017 IEEE 85th Vehicular Technology Conference (VTC Spring)*, IEEE, pp.1–5.

[12] **Abeywickrama, S.**, **Liu, L.**, **Chi, Y. and Yuen, C.** (2017). Over-the-air implementation of uplink NOMA, *GLOBECOM 2017-2017 IEEE Global Communications Conference*, IEEE, pp.1–6.

[13] **Gupta, A. and Jha, R.K.** (2015). A Survey of 5G Network: Architecture and Emerging Technologies, *IEEE Access*, *3*, 1206–1232.

[14] **Mohamad, M.**, **Nilsson, R. and van de Beek, J.** (2015). An Analysis of Out-of-band Emission and in-band Interference for Precoded and Classical OFDM Systems, *VDE 21th European Wireless Conference, 2015*, pp.1–5.

[15] **Baltar, L.G.**, **Waldhauser, D.S. and Nossek, J.A.**, (2007). Out-of-band Radiation in Multicarrier Systems: a Comparison, Multi-Carrier Spread Spectrum, Springer, pp.107–116.

[16] **Naima, S.**, **Tarek, B.F. and Fatima, D.** (2017). Compromise Between Spectral Efficiency and Interference Cancellation in OFDM System, *IEEE International Conference on Engineering & MIS (ICEMIS), 2017*, pp.1–7.

[17] **Brandes, S.**, **Cosovic, I. and Schnell, M.** (2006). Reduction of Out-of-band Radiation in OFDM Systems by Insertion of Cancellation Carriers, *IEEE Communications Letters*, *10*(6), 420–422.

[18] **Cosovic, I.**, **Brandes, S. and Schnell, M.** (2006). Subcarrier Weighting: A Method for Sidelobe Suppression in OFDM Systems, *IEEE Communications Letters*, *10*(6), 444–446.

[19] **Cosovic, I. and Mazzoni, T.** (2006). Suppression of Sidelobes in OFDM Systems by Multiple-choice Sequences, *European Transactions on Telecommunications*, *17*(6), 623–630.

[20] **Farhang-Boroujeny, B.** (2011). OFDM versus Filter Bank Multicarrier, *IEEE Signal Processing Magazine*, *28*(3), 92–112.

[21] **Wunder, G.**, **Jung, P.**, **Kasparick, M.**, **Wild, T.**, **Schaich, F.**, **Chen, Y.**, **Ten Brink, S.**, **Gaspar, I.**, **Michailow, N.**, **Festag, A.** *et al.* (2014). 5GNOW: Non-Orthogonal, Asynchronous Waveforms for Future Mobile Applications, *IEEE Communications Magazine*, *52*(2), 97–105.

[22] **Schaich, F. and Wild, T.** (2014). Waveform Contenders for 5G – OFDM vs. FBMC vs. UFMC, *6th International Symposium on Communications, Control and Signal Processing (ISCCSP), 2014*, pp.457–460.

[23] **Schmidl, T.M. and Cox, D.C.** (1997). Robust Frequency and Timing Synchronization for OFDM, *IEEE Transactions on Communications*, *45*(12), 1613–1621.

[24] **Proakis, J.G.**, **Salehi, M.**, **Zhou, N. and Li, X.** (1994). *Communication systems engineering*, volume 2, Prentice Hall New Jersey.

[25] **Bellanger, M.**, **Le Ruyet, D.**, **Roviras, D.**, **Terré, M.**, **Nossek, J.**, **Baltar, L.**, **Bai, Q.**, **Waldhauser, D.**, **Renfors, M.**, **Ihalainen, T.** *et al.* (2010). FBMC Physical Layer: A Primer, *PHYDYAS*, *25*(4), 7–10.

[26] **Schaich, F.** (2010). Filterbank Based Multi Carrier Transmission (FBMC) — Evolving OFDM: FBMC in the Context of WiMAX, *IEEE European Wireless Conference (EW), 2010*, pp.1051–1058.

[27] **Estella, I.**, **Pascual-Iserte, A. and Payaró, M.** (2010). OFDM and FBMC Performance Comparison for Multistream MIMO Systems, *Future Network and Mobile Summit, 2010*, pp.1–8.

[28] **Gaspar, I.S.**, **Mendes, L.L.**, **Michailow, N. and Fettweis, G.** (2014). A Synchronization Technique for Generalized Frequency Division Multiplexing, *EURASIP Journal on Advances in Signal Processing*, *2014*(1), 67.

[29] **Fettweis, G.**, **Krondorf, M. and Bittner, S.** (2009). GFDM - Generalized Frequency Division Multiplexing, *IEEE 69th Vehicular Technology Conference, 2009*, pp.1–4.

[30] **Michailow, N.**, **Matthé, M.**, **Gaspar, I.S.**, **Caldevilla, A.N.**, **Mendes, L.L.**, **Festag, A. and Fettweis, G.** (2014). Generalized Frequency Division Multiplexing for 5th Generation Cellular Networks, *IEEE Transactions on Communications*, *62*(9), 3045–3061.

[31] **Roessler, A.** (2016). 5G Waveform Candidates Application Note, *Rohde&Schwarz, Munich, Germany, Tech. Rep. 1MA271*.

[32] **de Almeida, I.B.F. and Mendes, L.L.** (2018). Linear GFDM: A Low Out-of-band Emission Configuration for 5G Air Interface, *2018 IEEE 5G World Forum (5GWF)*, IEEE, pp.311–316.

[33] **Zhang, X.**, **Jia, M.**, **Chen, L.**, **Ma, J. and Qiu, J.** (2015). Filtered-OFDM-Enabler for Flexible Waveform in the 5th Generation Cellular Networks, *IEEE Global Communications Conference (GLOBECOM), 2015*, pp.1–6.

[34] **Abdoli, J.**, **Jia, M. and Ma, J.** (2015). Filtered OFDM: A New Waveform for Future Wireless Systems, *IEEE 16th International Workshop on Signal Processing Advances in Wireless Communications (SPAWC), 2015*, pp.66–70.

[35] **Zhang, L.**, **Ijaz, A.**, **Xiao, P.**, **Molu, M.M. and Tafazolli, R.** (2018). Filtered OFDM Systems, Algorithms, and Performance Analysis for 5G and Beyond, *IEEE Transactions on Communications*, *66*(3), 1205–1218.

[36] **Gerzaguet, R.**, **Bartzoudis, N.**, **Baltar, L.G.**, **Berg, V.**, **Doré, J.B.**, **Kténas, D.**, **Font-Bach, O.**, **Mestre, X.**, **Payaró, M.**, **Färber, M.** *et al.* (2017). The 5G Candidate Waveform Race: A Comparison of Complexity and Performance, *EURASIP Journal on Wireless Communications and Networking*, *2017*(1), 13.

[37] **Yunzheng, T.**, **Long, L.**, **Shang, L. and Zhi, Z.** (2015). A Survey: Several Technologies of Non-Orthogonal Transmission for 5G, *China communications*, *12*(10), 1–15.

[38] **Helwa, S.S.**, **Ibrahim, M. and Elramly, S.** (2016). Universal Filtered Multi-carrier Performance Analysis with Multipath Fading Channels, *IEEE 10th International Conference on Next Generation Mobile Applications, Security and Technologies (NGMAST), 2016*, pp.35–40.

[39] **Malmgren, G.** (1996). Impact of Carrier Frequency Offset, Doppler Spread and Time Synchronisation Errors in OFDM based Single Frequency Networks, *IEEE Global Telecommunications Conference, 1996*, volume 1, pp.729–733.

[40] **Ma, X.**, **Kobayashi, H. and Schwartz, S.C.** (2003). Effect of Frequency Offset on BER of OFDM and Single Carrier Systems, *14th IEEE Proceedings on Personal, Indoor and Mobile Radio Communications (PIMRC), 2003*, volume 3, pp.2239–2243.

[41] **Wang, X.**, **Wild, T. and Schaich, F.** (2015). Filter Optimization for Carrier Frequency and Timing Offset in Universal Filtered Multi-carrier Systems, *IEEE 81st Vehicular Technology Conference (VTC), 2015*, pp.1–6.

[42] **Jafri, A.R.**, **Majid, J.**, **Shami, M.A.**, **Imran, M.A. and Najam-Ul-Islam, M.** (2017). Hardware Complexity Reduction in Universal Filtered Multicarrier Transmitter Implementation, *IEEE Access*, *5*, 13401–13408.

[43] **Li, Y.**, **Tian, B.**, **Yi, K. and Yu, Q.** (2017). A Novel Hybrid CFO Estimation Scheme for UFMC-based Systems, *IEEE Communications Letters*, *21*(6), 1337–1340.

[44] **Chen, X.**, **Wu, L.**, **Zhang, Z.**, **Dang, J. and Wang, J.** (2018). Adaptive Modulation and Filter Configuration in Universal Filtered Multi-Carrier Systems, *IEEE Transactions on Wireless Communications*, *17*(3), 1869–1881.

[45] **Wen, J.**, **Hua, J.**, **Lu, W.**, **Zhang, Y. and Wang, D.** (2018). Design of Waveform Shaping Filter in the UFMC System, *IEEE Access*.

[46] **Vakilian, V.**, **Wild, T.**, **Schaich, F.**, **ten Brink, S. and Frigon, J.F.** (2013). Universal-Filtered Multi-Carrier Technique for Wireless Systems Beyond LTE, *IEEE Globecom Workshops, 2013*, pp.223–228.

[47] **Wu, M.**, **Dang, J.**, **Zhang, Z. and Wu, L.** (2018). An Advanced Receiver for Universal Filtered Multi-Carrier, *IEEE Vehicular Technology Society*.

[48] **Reiners, C. and Rohling, H.** (1994). Multicarrier Transmission Technique in Cellular Mobile Communications Systems, *IEEE 44th Vehicular Technology Conference, 1994*, pp.1645–1649.

[49] **Cvijetic, N.** (2012). OFDM for Next-Generation Optical Access Networks, *Journal of Lightwave Technology*, *30*(4), 384–398.

[50] **Mabrouk, M.B.**, **Chafii, M.**, **Louet, Y. and Bader, F.** (2017). A Precoding-based PAPR Reduction Technique for UF-OFDM and Filtered-OFDM Modulations in 5G Systems, *23th European Wireless Conference on European Wireless, 2017*, pp.1–6.

[51] **Wild, T.**, **Schaich, F. and Chen, Y.** (2014). 5G Air Interface Design Based on Universal Filtered (UF-) OFDM, *19th International Conference on Digital Signal Processing (DSP), 2014*, pp.699–704.

[52] **Dore, J.B.**, **Gerzaguet, R. and Ktenas, D.** (2016). 5G Cellular Networks with Relaxed Synchronization: Waveform Comparison and New Results, *IEEE 83rd Vehicular Technology Conference (VTC Spring), 2016*, pp.1–5.

[53] **Wang, X.**, **Schaich, F. and ten Brink, S.** (2014). Channel Estimation and Equalization for 5G Wireless Communication Systems, *University of Stuttgart*.

[54] **Brandes, S.**, **Cosovic, I. and Schnell, M.** (2010). Techniques for Reducing Out-of-Band Radiation in OFDM based Transmission Systems, *Transactions on Emerging Telecommunications Technologies*, *21*(2), 142–153.

[55] **Shen, Y. and Martinez, E.** (2006). Channel Estimation in OFDM Systems, *Freescale Semiconductor Application Note*, 1–15.

[56] **Schaich, F.**, **Wild, T. and Chen, Y.** (2014). Waveform Contenders for 5G–Suitability for Short Packet and Low Latency Transmissions, *IEEE 79th Vehicular Technology Conference (VTC Spring), 2014*, IEEE, pp.1–5.

[57] **Wang, X.**, **Ho, P. and Wu, Y.** (2005). Robust Channel Estimation and ISI Cancellation for OFDM Systems with Suppressed Features, *IEEE Journal on Selected Areas in Communications*, *23*(5), 963–972.

[58] **Clark, C.L.** (2005). *LabVIEW Digital Signal Processing*, Tata McGraw-Hill Education.

[59] **Url-1** <*http://www.ni.com/pdf/manuals/375867d.pdf*>, date retrieved 02.10.2018.

[60] **Url-2** <*http://www.ni.com/pdf/manuals/374193d.pdf*>, date retrieved 02.10.2018.

[61] **Ai, B.**, **Yang, Z.x.**, **Pan, C.y.**, **Ge, J.h.**, **Wang, Y. and Lu, Z.** (2006). On the Synchronization Techniques for Wireless OFDM Systems, *IEEE Transactions on Broadcasting*, *52*(2), 236–244.

[62] **Kaur, S.**, **Singh, H. and Sappal, A.S.** (2012). Carrier Frequency Offset Estimation for OFDM Systems Using Time/Frequency-Domain Techniques, *International Journal of Advanced Research in Computer Science and Electronics Engineering (IJARCSEE)*, *1*(2), pp–154.

[63] **Moose, P.H.** (1994). A Technique for Orthogonal Frequency Division Multiplexing Frequency Offset Correction, *IEEE Transactions on Communications*, *42*(10), 2908–2914.

[64] **Kaur, S.**, **Singh, C. and Sappal, A.S.** (2012). Effects and Estimation Techniques of Symbol Time Offset and Carrier Frequency Offset in OFDM System: Simulation and Analysis, *International Journal of Electronics and Computer Science Engineering*, 1188–1196.

[65] **Mahmoud, H.A. and Arslan, H.** (2009). Error Vector Magnitude to SNR Conversion for Nondata-Aided Receivers, *IEEE Transactions on Wireless Communications*, *8*(5).

[66] **Uluocak, S. and Başar, E.** (2017). Spatial modulation for multi-user massive MIMO systems, *2017 25th Signal Processing and Communications Applications Conference (SIU)*, pp.1–4.

[67] **Rajashekar, R.**, **Hari, K.V.S. and Hanzo, L.** (2013). Antenna Selection in Spatial Modulation Systems, *IEEE Communications Letters*, *17*(3), 521–524.

[68] **Sun, Z.**, **Xiao, Y.**, **Yang, P.**, **Li, S. and Xiang, W.** (2017). Transmit Antenna Selection Schemes for Spatial Modulation Systems: Search Complexity Reduction and Large-Scale MIMO Applications, *IEEE Transactions on Vehicular Technology*, *66*(9), 8010–8021.

[69] **Ntontin, K.**, **Renzo, M.D.**, **Perez-Neira, A.I. and Verikoukis, C.** (2013). A Low-Complexity Method for Antenna Selection in Spatial Modulation Systems, *IEEE Communications Letters*, *17*(12), 2312–2315.

[70] **Li, H.**, **Song, L. and Debbah, M.** (2014). Energy Efficiency of Large-Scale Multiple Antenna Systems with Transmit Antenna Selection, *IEEE Transactions on Communications*, *62*(2), 638–647.

[71] **Ni, Y.**, **Zhang, W. and Chen, M.** (2013). Antenna subset selection in MU large-scale MIMO systems, *2013 International Conference on Wireless Communications and Signal Processing*, pp.1–5.

[72] **Qu, W.**, **Zhang, M.**, **Cheng, X. and Ju, P.** (2017). Generalized Spatial Modulation With Transmit Antenna Grouping for Massive MIMO, *IEEE Access*, *5*, 26798–26807.

[73] **Serafimovski, N.**, **Younis, A.**, **Mesleh, R.**, **Chambers, P.**, **Di Renzo, M.**, **Wang, C.X.**, **Grant, P.M.**, **Beach, M.A. and Haas, H.** (2013). Practical implementation of spatial modulation, *IEEE Trans. Veh. Technol.*, *62*(9), 4511–4523.

[74] **Goztepe, C. and Kurt, G.K.** (2019). The impact of out of band emissions: A measurement based performance comparison of UF-OFDM and CP-OFDM, *Physical Communication*.

[75] **Patcharamaneepakorn, P.**, **Wu, S.**, **Wang, C.**, **Aggoune, E.M.**, **Alwakeel, M.M.**, **Ge, X. and Renzo, M.D.** (2016). Spectral, Energy, and Economic Efficiency of 5G Multicell Massive MIMO Systems With Generalized Spatial Modulation, *IEEE Trans. Veh. Tech.*, *65*(12), 9715–9731.

[76] **Gao, X.**, **Edfors, O.**, **Tufvesson, F. and Larsson, E.G.** (2015). Massive MIMO in Real Propagation Environments: Do All Antennas Contribute Equally?, *IEEE Trans. Commun.*, *63*(11), 3917–3928.

[77] **Rajashekar, R.**, **Hari, K.V.S. and Hanzo, L.** (2013). Antenna Selection in Spatial Modulation Systems, *IEEE Commun. Lett.*, *17*(3), 521–524.

[78] **Joung, J.** (2016). Machine Learning-Based Antenna Selection in Wireless Communications, *IEEE Commun. Lett.*, *20*(11), 2241–2244.

[79] **He, D.**, **Liu, C.**, **Quek, T.Q.S. and Wang, H.** (2018). Transmit Antenna Selection in MIMO Wiretap Channels: A Machine Learning Approach, *IEEE Wireless Commun. Lett.*, *7*(4), 634–637.

[80] **Qu, W.**, **Zhang, M.**, **Cheng, X. and Ju, P.** (2017). Generalized Spatial Modulation With Transmit Antenna Grouping for Massive MIMO, *IEEE Access*, *5*, 26798–26807.

[81] **Datta, T. and Chockalingam, A.** (2013). On generalized spatial modulation, *Proc. IEEE WCNC*, pp.2716–2721.

[82] **Mesleh, R. and Alhassi, A.** (2018). *Space Modulation Techniques*, volume288, Wiley Online Library.

[83] **Nosrat-Makouei, B.**, **Andrews, J.G. and Heath, R.W.** (2011). MIMO Interference Alignment Over Correlated Channels With Imperfect CSI, *IEEE Trans. Signal Process.*, *59*(6), 2783–2794.

[84] **Sadek, M.**, **Tarighat, A. and Sayed, A.H.** (2004). Exploiting spatio-temporal correlation for rate-efficient transmit beamforming, *Conf. Rec. the 38th Asilomar Conf. Signals, Syst. and Comput., 2004.*, pp.2027–2031.

[85] **Alpaydin, E.** (2010). *Introduction to Machine Learning*, The MIT Press, 2nd edition.

[86] **Géron, A.** (2017). *Hands-On Machine Learning with Scikit-Learn and TensorFlow*, O'Reilly Media.

[87] **Hastie, T.**, **Tibshirani, R. and Friedman, J.** (2001). *The Elements of Statistical Learning*, Springer New York Inc.

APPENDICES

APPENDIX A : Generalized Spatial Modulation Transmitter Block Diagram.
APPENDIX B : CP-OFDM with NOMA Transmitter Block Diagram.
APPENDIX C : Spatial Modulation Receiver Block Diagram.
APPENDIX D : UF-OFDM Transmitter Block Diagram.

APPENDIX A

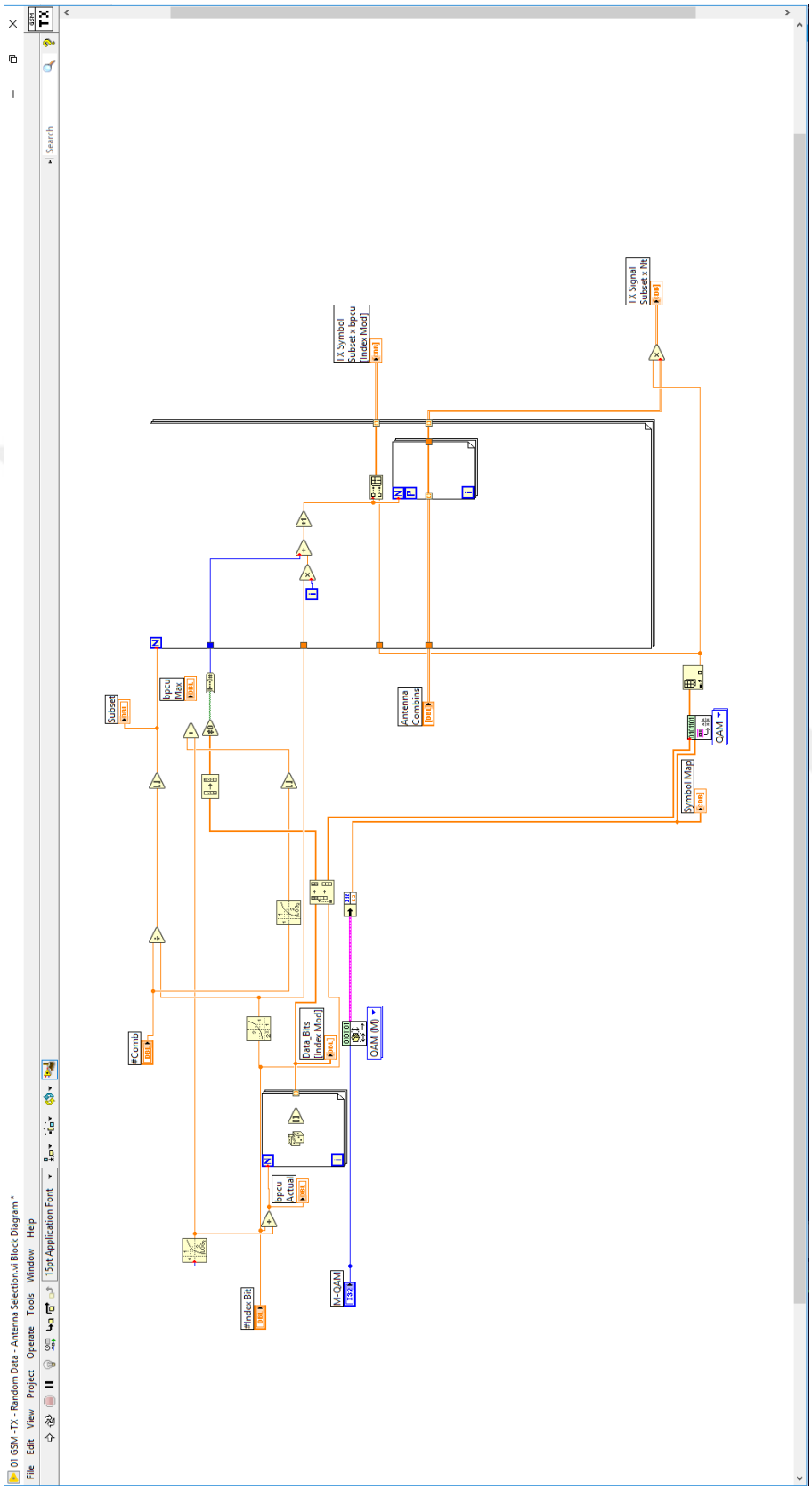

Figure A : Generalized spatial modulation transmitter block diagram.

APPENDIX B

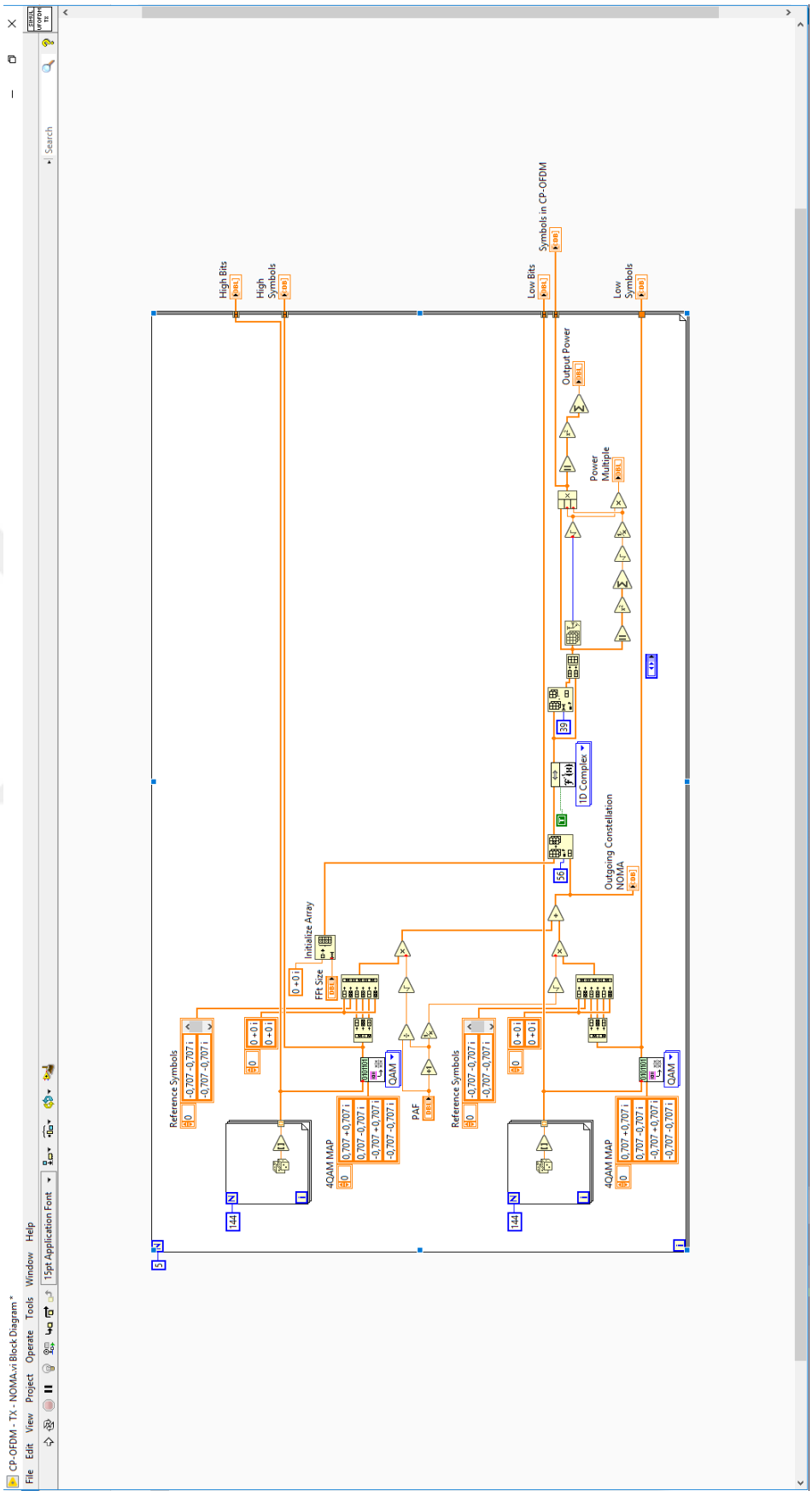

Figure B : CP-OFDM with NOMA transmitter block diagram.

APPENDIX C

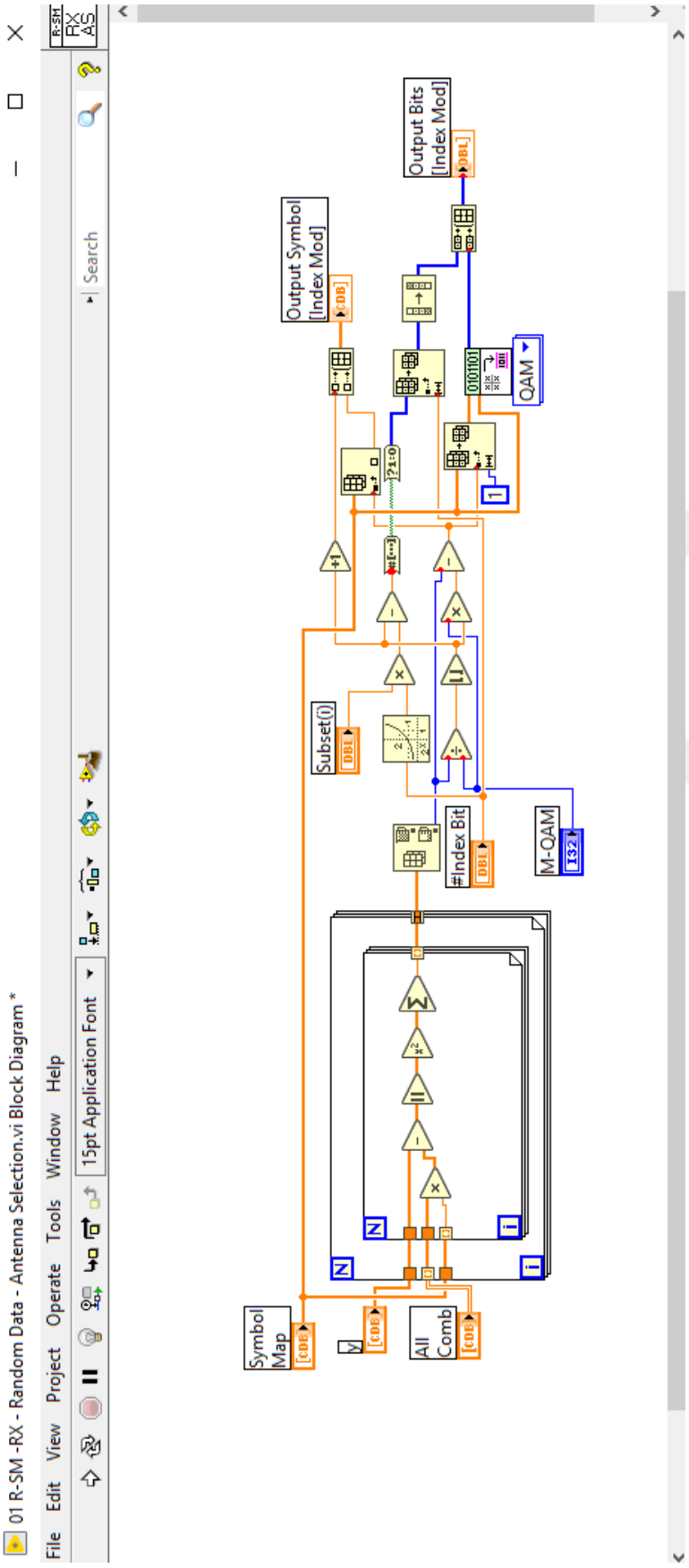

Figure C : Spatial modulation receiver block diagram.

APPENDIX D

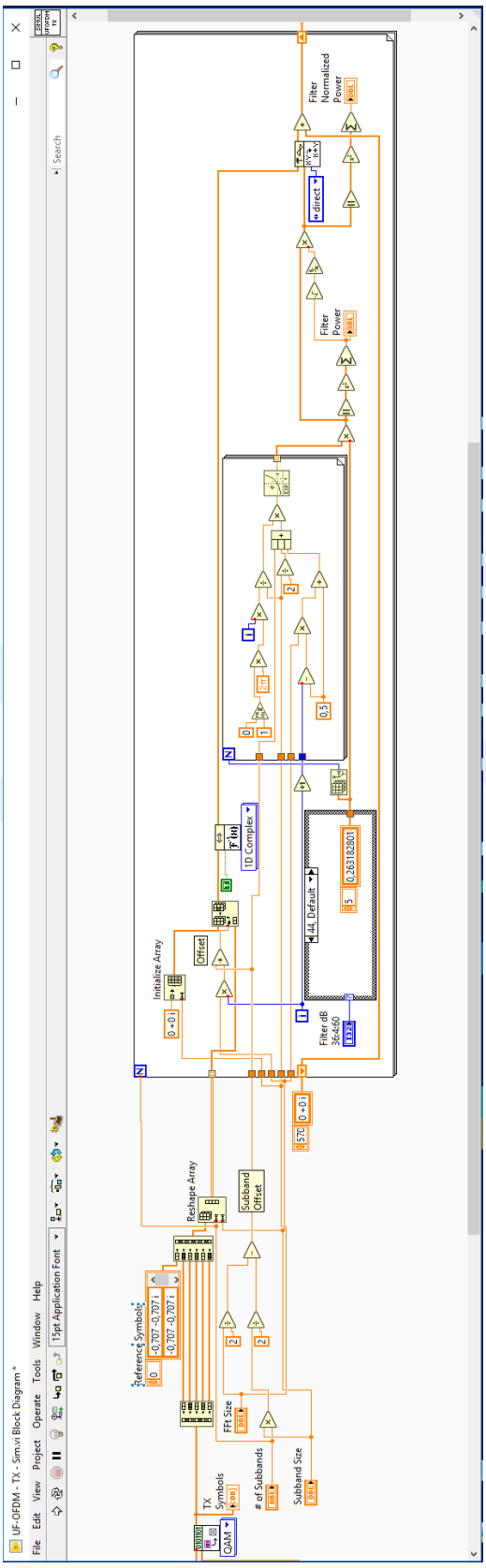

Figure D : UF-OFDM transmitter block diagram.

CURRICULUM VITAE

Name Surname: Caner Göztepe

Place and Date of Birth: Manisa 08.02.1991

E-Mail: goztepe@itu.edu.tr

EDUCATION:

- **B.Sc.:** 2017, Istanbul Technical University, Faculty of Electrical and Electronics Engineering, Telecommunication Engineering.

PROFESSIONAL EXPERIENCE AND REWARDS:

- 2016-2018: COREDE Software and Technology Inc., Project Manager (PM).
- 2018-Now: Istanbul Technical University Wireless Communication Research Laboratory, Researcher.
- 2018-Now: iCodion Software and Technology Inc., PM.

PUBLICATIONS, PRESENTATIONS AND PATENTS ON THE THESIS:

- Goztepe, C., Kurt, G. K. (2019). The impact of out of band emissions: A measurement based performance comparison of UF-OFDM and CP-OFDM. *Physical Communication*, 33, 78-89.
- Gecgel, S., Goztepe, C. and Kurt, G.K. (2019). Antenna Selection on Spatial Modulation: A Machine Learning Approach, *2019 27th Signal Processing and Communications Applications Conference (SIU)*, IEEE, pp.1–4.
- Durmaz, M.A., Goztepe, C., Kurt, G.K., Tokaz, M. and Kucur, O. (2019). Non-Orthogonal Multiple Access System Implementation in Software Defined Radios, *2019 27th Signal Processing and Communications Applications Conference (SIU)*, IEEE, pp.1–4.
- Gecgel, S., Goztepe, C., Kurt, G. K. (2019). Transmit Antenna Selection for Massive MIMO GSM with Machine Learning. arXiv preprint arXiv:1903.04460.
- Gecgel, S., Goztepe, C. and Kurt, G.K. (2019). Jammer Detection based on Artificial Neural Networks: A Measurement Study, *Proceedings of the ACM Workshop on Wireless Security and Machine Learning*, ACM, pp.43–48.

OTHER PUBLICATIONS, PRESENTATIONS AND PATENTS:

- Gecgel, S., Goztepe, C., Kurt, G. K. (2019). Transmit Antenna Selection for Massive MIMO GSM with Machine Learning. *Wireless Communication Letter*, Under Review.